Research Square

Preprints are preliminary reports that have not undergone peer review.
They should not be considered conclusive, used to inform clinical practice,
or referenced by the media as validated information.

A novel thermosensitive K2P channel with TREK-like properties in the neuroendocrine system of Procambarus clarkii

Juan Manuel Hernández-Martínez
Centro de Investigación y de Estudios Avanzados del Instituto Politécnico Nacional
Iván Uriel Valladares-Hernández
Escuela Nacional Escuela Nacional de Ciencias Biológicas, Unidad Profesional Adolfo López Mateos del IPN
Itzel Scarlett Moreno-Ramírez
Centro de Investigación y de Estudios Avanzados del Instituto Politécnico Nacional
Kattia Yamilet Moreno-Velázquez
Centro de Investigación y de Estudios Avanzados del Instituto Politécnico Nacional
Edith Sánchez-Jaramillo
Instituto Nacional de Psiquiatría Ramón de la Fuente Muñiz
Juan Manuel Arias
Universidad Nacional Autónoma de México
Ubaldo García-Hernández
ubaldo.garcia@cinvestav.mx

Centro de Investigación y de Estudios Avanzados del Instituto Politécnico Nacional

Research Article

Keywords:

Posted Date: October 22nd, 2026

DOI: https://doi.org/10.21203/rs.3.rs-11273270/v1

License: This work is licensed under a Creative Commons Attribution 4.0 International License.
Read Full License

Additional Declarations: No competing interests reported.

Abstract

Two-pore domain potassium (K_{2P}) channels regulate resting membrane potential and neuronal excitability by mediating background K^+ currents. Their modulation by physical and chemical stimuli, including temperature, remains poorly characterized in invertebrate neuroendocrine systems. Here, we identified, cloned, and functionally characterized $PcK_{2P}1$, a thermosensitive channel from the crayfish *Procambarus clarkii*. In X-organ neurons, warming from 17 to 27°C enhanced background K^+ currents approximately threefold, hyperpolarized the membrane, and suppressed spontaneous firing. Transcriptome analysis identified a sequence encoding a 417-amino-acid protein with two potassium selectivity filter motifs and four transmembrane helices, preserving canonical K_{2P} topology despite low sequence identity with human TREK-2 (~ 29%). Heterologous expression in HEK293T cells produced outwardly rectifying K^+ currents with reversal potentials that shifted with extracellular K^+ concentration. Single-channel recordings revealed two conductance states of 40.86 and 106.6 pS. Warming from 20 to 30°C increased macroscopic currents with a Q_{10} of approximately 2.4 and enhanced open probability with Q_{10} values of 3.3–3.6, without significantly changing mean open time. $PcK_{2P}1$ was activated by membrane stretch and arachidonic acid and inhibited by Mg^{2+} and tetrahexylammonium, whereas tetraethylammonium produced only modest inhibition at positive potentials. Fluorescence in situ hybridization confirmed $PcK_{2P}1$ mRNA expression in X-organ neurons. These findings identify $PcK_{2P}1$ as a thermosensitive, polymodal K_{2P} channel with TREK-like properties and suggest a contribution to temperature-dependent regulation of excitability in an invertebrate neuroendocrine system.

Significance statement

This study addresses an underexplored question regarding the molecular basis of thermosensation in an invertebrate neuroendocrine system. The identification of a novel thermosensitive K_{2P} channel extends our understanding of leak channel function beyond vertebrate systems. The experimental approach integrates molecular biology, bioinformatics, electrophysiology, pharmacology, and fluorescence *in situ* hybridization.

Introduction

Temperature is one of the most influential environmental factors affecting the physiology of decapod crustaceans (Payette and McGaw, 2003; Luo et al., 2022), requiring neuroendocrine adaptations to maintain homeostasis (Wang et al, 2025). Central to this response is the X-organ–sinus gland (XO-SG) neurosecretory system located within the eyestalks. This system is composed of discrete populations of neurons that regulate numerous physiological functions, including metabolism, molting (ecdysis), reproduction, ionic/osmotic balance, and pigmentation changes (García and Aréchiga, 1998; Chung et al. 2010). For instance, thermal stress is known to stimulate neuroendocrine responses of the XO-SG system, such as the secretion of crustacean hyperglycemic hormone (CHH), leading to hyperglycemia as part of the physiological adaptation (Chung and Zmora, 2008). These observations highlight the

importance of temperature detection in this neuroendocrine system. Although the molecular thermosensors responsible for temperature detection in the XO-SG system remain unknown, an ortholog of the transient receptor potential ankyrin subtype 1 (TRPA1), which contributes to heat sensing and modulates immune responses has been described in the crayfish *Procambarus clarkii* (Liu et al., 2022).

Temperature governs metabolism through its effects on the rates of biochemical reactions (Gillooly et al., 2001). The temperature dependence of biological processes is traditionally expressed as the temperature coefficient (Q_{10}). In fact, temperature-sensitive ion channels are characterized by a pronounced temperature dependence, typically exhibiting Q_{10} values greater than 3 (Brauchi et al., 2004; Lamas et al., 2019). Among temperature-sensitive ion channels, the TREK subfamily of two-pore domain potassium (K_{2P}) channels has emerged as a key regulator of neural thermosensation in mammalian hypothalamic circuits, exhibiting Q_{10} values close to 7 (Maingret et al., 2000). These background potassium channels act as tonic regulators of neuronal excitability in temperature-sensitive neurons (Noël et al., 2009).

K_{2P} channels differ from other K^+ channels in their topology, gating behavior, and functional properties. Each subunit contains two pore-forming domains and four transmembrane segments, and functional channels arise through dimerization (Enyedi and Czirják, 2010; Lotshaw, 2007; Coetzee et al., 1999). These channels function primarily as leak channels, contributing to the resting membrane potential and dampening neural excitability by maintaining it close to the K^+ equilibrium potential (Honoré, 2007). In addition, they display relatively large single-channel conductance values, with multiple conductance states arising from isoform-specific properties and heteromeric assembly (Lotshaw, 2007; Li et al., 2006; Simkin et al., 2008; Enyedi and Czirják, 2010).

The TREK subfamily, comprising TREK-1, TREK-2, and TRAAK channels, is the only known K_{2P} subfamily that displays robust temperature-dependent activation in both the mammalian nervous system and in heterologous expression systems (Maingret et al., 2000; Kang et al., 2005). Furthermore, TREK channel activity is regulated by a wide variety of stimuli, acting as polymodal integrators responsive to mechanical stretch, voltage, pH, lipids, phosphorylation pathways, polyunsaturated fatty acids, volatile anesthetics, and temperature (Patel et al., 1998; Lesage et al., 2000; Bockenhauer et al., 2001; Maingret et al., 2002; Murbartián et al., 2005; Chemin et al., 2005, 2007; Cohen et al., 2008; Sandoz et al., 2009; Schewe et al., 2016; Lamas et al., 2019). Although this channel family is remarkably extensive in invertebrates, it remains poorly classified, and its electrophysiological properties, as well as its contribution to thermosensation, remain largely unexplored.

In this study, using transcriptomic data, we identified, cloned and characterized a K_{2P} channel subunit from the *P. clarkii* eyestalk with TREK-like properties. This channel, named $PcK_{2P}1$, displays thermosensitivity when heterologously expressed in HEK293T cells. Using bioinformatic analyses and electrophysiological characterization, we demonstrate that $PcK_{2P}1$ exhibits conserved K_{2P} topology, predicted regulatory motifs, and electrophysiological properties closely resembling those of mammalian

TREK channels. Furthermore, we show that $PcK_{2P}1$ is expressed in the neurosecretory XO-SG system, where it could regulate neuronal excitability and contribute to temperature-dependent physiological and behavioral responses.

Materials and Methods

Animals. P. clarkii were obtained from the dam San Luis Taxhimay (Estado de México, México). Animals were maintained for two weeks under a 12:12 h light/dark cycle at room temperature (22–26°C) and fed *ad libitum* with carrot slices and fish pellets. All procedures involving *P. clarkii* were approved by the Animal Care Committee of CINVESTAV. The handling and euthanasia of experimental animals were carried out in accordance with the guidelines established by the National Institutes of Health (NIH Guide for the Care and Use of Laboratory Animals, Publication No. 8023, revised 1978) and the Mexican Official Standard for Animal Care (NOM-062-ZOO-1999). All experiments were performed using adult organisms. Prior to any manipulation, animals were anesthetized on triturate ice for 20 min. The excised eyestalks were placed in cooled crayfish saline solution with the following composition (in mM): 205 NaCl, 5.4 KCl, 13.5 $CaCl_2$, 2.6 $MgCl_2$, and 10 HEPES (pH 7.4, adjusted with NaOH). The exoskeleton and surrounding connective tissue of the eyestalks were carefully removed. The X-organ was then dissected and either transferred to a homogenizer for RNA extraction, fixed for *in situ* hybridization, or used for primary cell culture, as described below.

Identification of K_{2P}-like subunits sequences. Using the tBLASTn algorithm and querying with the TREK-1 (*Rattus norvegicus*, accession number NP_742038.2) and Twk-18 (*Caenorhabditis elegans*, accession number NP_509516.1) sequences in the *P. clarkii* Transcriptome Shotgun Assembly (TSA) (Manfrin et al., 2015; Tom et al., 2014), the sequence Pc_6896 was identified as an RNA transcript encoding a putative K_{2P} subunit with similarities to other K_{2P} sequences. The identified sequence was named $PcK_{2P}1$, based on its molecular and functional similarities to K_{2P} subunits.

Bioinformatic analysis. Sequence analysis was performed using ApE software (UT, USA) to identify potential open reading frames (ORFs; Davis & Jorgensen, 2022), and Clustal Omega (EMBL-EBI) to conduct multiple sequence alignment and generate the identity matrix. Transmembrane topology was predicted with DeepTMHMM 1.0 (Hallgren et al., 2022). Potential N- and O-glycosylation sites were identified using NetNGlyc 1.0 (Gupta et al., 1999) and DictyOGlyc 1.1 (Gupta & Brunak, 2002), respectively. Phosphorylation sites were predicted using the NetPhos 3.1 server (Blom et al., 1999). Subcellular localization and membrane association of the PcK2P1 sequence were predicted with DeepLoc 2.1 (Ødum et al., 2024). Protein structure homology modeling was carried out using SWISS-MODEL (Waterhouse et al., 2018). Phylogenetic analysis was conducted with MEGA X software (Molecular Evolutionary Genetics Analysis; PA, USA) using the Maximum Likelihood method and the JTT matrix-based model (Jones et al., 1992). Neighbor-Joining and BioNJ algorithms were applied to a matrix of pairwise distances estimated with the JTT model, and the topology with the highest log-likelihood value was selected. Amino acid sequences for K_{2P} subunits from vertebrate and invertebrate

organisms were obtained from the National Center for Biotechnology Information (NCBI) database and used to construct the phylogenetic tree: *Aplysia californica* AcK2p1 (AAN62847.1), AcK2p2 (DQ166529.1); *Caenorhabditis elegans* TWK-18 (AAC32861.1); *Drosophila melanogaster* TASK-6 (NP_001262539.1), ORK1 (NP_727466.1); *Mus musculus* TASK-1 (NP_034738.1), TRESK (NP_997144.1); and *Homo sapiens* TRAAK (Q9NYG8.2), TREK-1 (O95069.2), TREK-2 (P57789.1), THIK-1 (NP_071337.2), TWIK-1 (NP_002236.1), and TALK-1 (Q96T55.1). In this study, the name of each subunit contains the initial letters of the species name, followed by the common name of the K_{2P} channel.

RNA extraction, molecular cloning, and constructs. The X-organ, medulla terminalis, medulla interna, and medulla externa ganglia were dissected from ten eyestalks, along with abdominal muscle tissue, to extract the total RNA using the TRIzol protocol (Green and Sambrook, 2012). The above helped to determine the expression pattern of $PcK_{2P}1$ in different regions of eyestalk. Primers for $PcK_{2P}1$ were designed with Clone Manager 9 software (Scientific & Educational Software, NC, USA) (Table 1). First-strand cDNA was synthesized using ProtoScript II reverse transcriptase (New England Biolabs Inc., MA, USA) in a 20 µL reaction containing the $d(T)_{18}$ linker reverse-1 primer (r1) primers (60 µM each), 1x reaction buffer, RiboLock RNase inhibitor (2 U/µL), and 1.5 µg of total RNA. The reaction mixture was incubated at 42°C for 1 h, followed by enzyme inactivation at 80°C for 5 min and cooling to 4°C. The resulting cDNA was diluted with nuclease-free water to a final volume of 100 µL and stored at − 20°C until use. PCR amplifications were carried out in 25 µL reactions containing 0.8 mM dNTPs, 0.4 µM forward and reverse primers each, 0.5 U Q5 DNA polymerase (New England Biolabs Inc., MA, USA), and 5 µL of cDNA. Amplicons were verified by restriction analysis and cloned into the pJET1.2/blunt vector (CloneJET PCR Cloning Kit, Thermo Scientific, CA, USA) for sequencing. Full-length $PcK_{2P}1$ cDNA was subcloned into the bicistronic pIRES2–EGFP vector (Clontech Laboratories, CA, USA). To evaluate $PcK_{2P}1$ differential expression in crayfish eyestalk tissues, 5 µL of cDNA obtained from each region was used as template for PCR, following the protocol of Jiménez-Vázquez et al. (2016).

PcK2P1f2–pcK2P1r2 primer pair was used to amplify $PcK_{2P}1$. The PcGABAAβf–$PcGABA_A$βr and PcGAPDHf2–PcGAPDHr2 primer pairs were used to amplify *P. clarkii* $PcGABA_A$β (accession No. KM115031) and glyceraldehyde-3-phosphate dehydrogenase (GAPDH; accession No. AB094145.1), respectively. $PcGABA_A$β served as a positive control, whereas GAPDH was used as a reference gene.

Table 1
Primers designed for $PcK_{2P}1$ amplification. Primers were identified with f for forward and r for reverse, according to its localization in the sequence.

Subunit	Primers
$PcK_{2P}1$	PcK2P1f1 - GCAGCATCAAAGACCTCTAC
	PcK2P1f2 - CGGCCTACAAGTTATCCAC
	PcK2P1r1 - GAATTCTGCGGGTTTATGCATTCG
	PcK2P1r2 - GAATTCCACTGCACTACTTAGCTCTC
$PcGABA_A\beta$	PcGABA2βf - ATGGACCGACAGCTCTGCATCAT
	PcGABA2βr - CGGCGTATTCAAGCAGCGAAGC
PcGAPDH	PcGAPDHf2 - TGCTCCTGTTGCGAAAGTC
	PcGAPDHr2 - CCCAAACTCGTTGTCATACC

cRNA probes for in situ hybridization. cRNA probes were generated using a PCR-modified pGEM-T Easy cloning vector (Promega) containing XhoI and XbaI restriction sites, following the protocol described by Jiménez-Vázquez et al. (2016). A $PcK_{2P}1$ fragment (493 bp), corresponding to the 5' end of the coding sequence and flanked by XhoI and XbaI sites, was subcloned into the plasmid. The pGEM-T-PcK2P1 plasmid was linearized with the appropriate restriction enzyme and used as a template for *in vitro* transcription. Digoxigenin-labeled sense and antisense riboprobes were synthesized using T7 and SP6 RNA polymerases, respectively, according to the manufacturer's instructions (DIG RNA Labeling Kit, SP6/T7; Roche, USA, Cat. No. 11175025910).

Fluorescent in situ hybridization (FISH). Following the procedure described by Sánchez-Jaramillo et al. (2022), eyestalks from *P. clarkii* were fixed in 4% paraformaldehyde in 0.1 M phosphate-buffered saline (PBS, pH 7.4) for 20 h and subsequently incubated in 25% sucrose for 24 h. Longitudinal sections of the eyestalk (20 µm thick) were then obtained, rinsed in 0.1 M PBS, mounted on Fisherbrand Superfrost Plus slides, and stored at − 80°C. Previous to hybridization, slides were rinsed in 1× PBS for 4 min, treated with proteinase K (1 µg/mL) at 37°C for 10 min, post-fixed in 4% paraformaldehyde in 0.1 M PBS (pH 7.4) for 5 min, acetylated in 0.25% acetic anhydride in 0.1 M triethanolamine for 10 min, dehydrated through a graded ethanol series (80%, 95%, and 100%; 1 min each), treated with chloroform for 10 min, and partially rehydrated in 95% ethanol. Eyestalk sections were incubated with a hybridization mix containing either sense or antisense DIG-labeled riboprobe (100 ng/mL) in 80 µL of hybridization buffer composed of 50% formamide, 2× standard saline citrate (SSC), 1× Denhardt's solution, 10 mM dithiothreitol (DTT), 250 µg/mL single-stranded salmon sperm DNA, 10% dextran sulfate, and 10% sodium dodecyl sulfate (SDS). Slides were immediately sealed with parafilm coverslips and incubated at 54°C for 15 h. After coverslip removal, sections were rinsed in 1× SSC (0.15 M NaCl, 0.015 M sodium citrate) for 15 min at room temperature, digested with RNase A (25 µg/mL; Sigma, USA, Cat. No. 4875) for 1 h at 37°C, rinsed again

in 1× SSC for 15 min at room temperature, in 0.5× SSC for 15 min at 65°C, twice in 0.1× SSC for 30 min at 65°C, and once in 0.1× SSC for 5 min at room temperature. Sections were then treated with 0.5% H_2O_2 and 0.5% Triton X-100 in 0.1 M PBS, rinsed three times in 0.1 M PBS, incubated in 100 mM maleic acid with 150 mM NaCl (pH 7.5) for 10 min at room temperature, and blocked in 1% blocking reagent (Roche, USA, Cat. No. 11096176001). DIG-labeled probes were detected using a peroxidase-conjugated anti-digoxigenin antibody (1:100 dilution in 1% blocking reagent, incubated at 4°C for 65 h). Sections were rinsed three times with 0.1 M Tris, 0.15 M NaCl, and 0.05% Tween-20. Signal amplification was performed using the Tyramide Signal Amplification (TSA) Plus Biotin Kit (PerkinElmer, USA, Cat. No. NEL749B001KT) for 30 min with the biotin amplification reagent diluted 1:100 in 0.05 M Tris (pH 7.5) containing 0.01% H_2O_2.Biotin signal was detected using Alexa Fluor 488–conjugated streptavidin (1:1000 dilution in 1% blocking reagent; Invitrogen, USA, Cat. No. S32354). The fluorophore was excited at 488 nm and emission was collected between 500–550 nm. Finally, sections were rinsed in TNT buffer and cover slipped with Vectashield antifade mounting medium containing DAPI (Vector Laboratories, USA, Cat. No. H-2000). To assess hybridization specificity, both antisense and sense probes were tested; sense probes produced no detectable signal in eyestalk tissue. Confocal images were acquired with a Leica DMi8 confocal microscope (Leica Microsystems, Wetzlar, Germany). Images were processed and assembled using ImageJ software (NIH, Bethesda, MD, USA).

XO primary culture, HEK293T culture and transfection. In this work, we performed electrophysiological recordings from both X-organ cells and HEK 293T transfected cells. X-organ cells were dissociated as follows: isolated X-organs were incubated with 80 µg/mL collagenase–dispase (Roche, Mannheim, Germany) in modified Leibovitz L-15 medium (Gibco/BRL, Grand Island, NY) for 30 min, following the protocol described for leech Retzius cells by García et al. (1990). The enzyme was removed by rinsing the tissue with L-15 medium, and X-organ cells were dissociated mechanically by suction using polished glass micropipettes. Dissociated cells were plated into recording chambers precoated with concanavalin A type III (Sigma-Aldrich, St. Louis, MO). The modified L-15 culture medium was prepared by adding 67.5 mM NaCl, 0.8 mM $MgCl_2$, 12.27 mM $CaCl_2$, 5.55 mM glucose, 2 mM L-glutamine, 10 mM HEPES, 5 mg/mL streptomycin, 5 U/mL penicillin (all from Sigma-Aldrich), and 16 µg/mL gentamicin (Schering-Plough, Mexico City, Mexico) to L-15 medium. Human Embryonic Kidney (HEK293T) cells (ATCC, CRL-1573) were maintained in Dulbecco's Modified Eagle Medium (DMEM; Gibco, NY, USA, Cat. No. 12100038) supplemented with 10% fetal bovine serum (BioWest, FL, USA, Cat. No. S1810-500), 3.7 g/L $NaHCO_3$, and 1% (v/v) antibiotic–antimycotic solution (Gibco, NY, USA, Cat. No. 15240096). Cells were incubated at 37°C in a 5% CO_2 incubator at 95% relative humidity. 35-mm culture dishes were used to place 1–3 × 10^6 cells for at least 3 days before transfection. For transfection, cells were treated with 1 µg of $PcK_{2P}1$ cDNA (cloned into the bicistronic pIRES2-EGFP vector) and 3 µg of PEI-Prime (Sigma-Aldrich, MO, USA, Cat. No. 919012), following the manufacturer's instructions. Between 24 and 72 h post-transfection, ~ 1 × 10^3 cells were replated into poly-L-lysine–coated recording chambers and incubated at 37°C for at least 2 h before electrophysiological recordings. Transfected cells were identified by EGFP fluorescence under epifluorescence microscopy.

Electrophysiology. Whole-cell voltage- and current-clamp recordings were performed from X-organ cells. Currents were acquired using an Axopatch 200B amplifier (Molecular Devices, CA, USA), digitized with a Digidata 1200 series interface (Molecular Devices, CA, USA) at a sampling rate of 10 kHz, and low-pass Bessel filtered at 5 kHz. Recording electrodes were fabricated from borosilicate glass capillaries (Sutter Instruments, Novato, CA) using a vertical pipette puller (Model 730, David Kopf Instruments). Electrodes were filled with internal solution containing (in mM): 207 KCl, 1 $MgCl_2$, 2 $CaCl_2$, 5 EGTA-Na, and 10 HEPES; the pH was adjusted to 7.4 with KOH. Pipette resistance was 5–10 MΩ. The external bath solution consisted of standard crayfish saline; (in mM): 205 NaCl, 5.4 KCl, 2.6 $MgCl_2$, 13.5 $CaCl_2$ and 10 HEPES; the pH was adjusted to 7.4 with NaOH. For symmetrical potassium experiments, NaCl was substituted for KCl in standard crayfish saline. Whole-cell recordings were performed using both current- and voltage-clamp protocols. In current-clamp mode, depolarizing and hyperpolarizing square pulses (± 0.1 nA, 250 ms) were applied at three bath temperatures (17, 22, and 27°C), with cells held at a membrane potential of − 50 mV. In voltage-clamp mode, I–V relationships were obtained using a square-pulse protocol from − 70 to + 70 mV in 10 mV steps (1 s duration) under symmetrical K^+ conditions, with a holding potential of 0 mV. In addition, cell-attached recordings were performed by applying a square pulse to − 50 mV to assess single-channel activity at the three temperatures.

HEK293T cells were recorded under voltage-clamp using both whole-cell and cell-attached configurations. Currents were acquired with an Axopatch 200A amplifier (Molecular Devices, CA, USA), digitized through a Digidata 1440A acquisition system (Molecular Devices, CA, USA) at a sampling rate of 10 kHz, and filtered with a low-pass Bessel filter at 5 kHz (whole-cell) or 2 kHz (cell-attached). Recording electrodes were the same as described above and were filled with an internal solution containing (in mM): 140 KCl, 2 $MgCl_2$, 5 EGTA-Na, and 10 HEPES; pH was adjusted to 7.4 with KOH. The standard physiological external solution contained (in mM): 140 NaCl, 5 KCl, 2 $MgCl_2$, 1 $CaCl_2$, and 10 HEPES; pH was adjusted to 7.4 with NaOH, although the primary external solution was symmetrical K^+ and contained (in mM): 145 KCl, 2 $MgCl_2$, 1 $CaCl_2$, and 10 HEPES; pH was adjusted to 7.4 with KOH. Additional intermediate K^+ solutions were identical to the symmetrical solution except that they contained (in mM): 105 NaCl and 40 KCl, or 35 NaCl and 110 KCl. Solutions were perfused at a rate of 2–3 mL/min. Currents were obtained in voltage-clamp mode using a voltage ramp either from − 140 to + 60 mV or from − 100 to 60 mV. For temperature-sensitivity recordings, the symmetrical solution was applied at 20, 25, and 30°C, according to the thermal preference of *P. clarkii*. The temperature was continuously monitored using a micro-thermistor positioned ~ 5 mm from the recorded cell. For Mg^{2+}-sensitivity assays, a symmetrical $MgCl_2$-free solution supplemented with 1 mM EDTA was used. For arachidonic acid (AA) modulation assays, a symmetrical solution supplemented with 10 µM AA was applied; AA was obtained from SIGMA and prepared from a 10 mM stock solution in ethanol and stored at − 20°C. Mechanical stimulation was applied during cell-attached recordings at − 80 mV and + 80 mV holding potentials under symmetrical K^+ conditions. Negative pressure (− 100 mmHg) was delivered through the patch-pipette to induce membrane stretch. Tetraethylammonium chloride (TEA) and tetrahexylammonium chloride (THexA) were obtained from SIGMA. Stock solutions (100 mM and 10 mM, respectively) were stored at − 20°C and diluted into the symmetrical recording solution to their final

concentrations. For cell-attached recordings, a square-pulse protocol from − 100 to + 100 mV in 10 mV steps (1 s duration) under symmetrical K^+ conditions was used; both pipette and bath solutions contained (in mM): 140 KCl, 2 $MgCl_2$, 5 EGTA-Na, and 10 HEPES; pH was adjusted to 7.4 with KOH. For single-channel analysis, the threshold for channel opening detection was set at 50%, and the filter dead time was 100 µs (0.3/cutoff frequency), such that events shorter than 50 µs were excluded. Data were analyzed to obtain conductance, mean open time, and open probability (Po) from amplitude and dwell-time histograms at a single conductance level, recorded at − 80 and + 80 mV. Each dataset was obtained from ~ 20 s of the current recording. For temperature-sensitivity experiments, temperature control of the external solutions was applied as described for whole-cell recordings. Single-channel analysis was performed as described above, and data were analyzed to obtain mean open time, relative open probability, and relative activity (NP_0, where N is the number of channels in the patch) from dwell-time histograms at a single conductance level, recorded at − 80 and + 80 mV. Each dataset was obtained from ~ 10 s of the current recording per temperature. Single-channel current traces shown in the figures were filtered at 1 kHz. Only recordings with a seal resistance > 1 GΩ were used for analysis. In whole-cell configuration, series resistance was 5–10 MΩ and compensated by ≥ 70%. Osmolarity of all HEK293T solutions was adjusted to 295–305 mOsm. Non-transfected HEK293T cells displayed no measurable currents under the same recording conditions. All electrophysiological data were analyzed using pClamp 10.6 software (Molecular Devices, CA, USA).

Statistical analysis. All data were analyzed and plotted using GraphPad Prism 8 (GraphPad Software, CA, USA) and Python libraries (NumPy, Pandas, and Matplotlib; version 3.8.5, Python Software Foundation). Values are expressed as mean ± SEM. The statistical tests applied to each dataset are indicated in the text. Whole-cell currents were normalized to the membrane capacitance of individual cells to account for differences in cell size.

Results

Temperature response of neuroendocrine X-organ neurons

Following optic peduncle ablation, the exoskeleton, muscles and connective tissue that cover the eyestalk were removed gently by microdissection under microscopic observation to expose the X-organ cell bodies. The experiments were made on a group of ~ 30 cells located in the most superficial layer of the X-organ. We previously showed that these neurons produce hyperglycemic hormone (Pérez-Polanco et al., 2011). The eyestalk preparation was mounted in a small volume recording chamber (200 µl) and continuously perfused with crayfish saline solution for 1 h before experimental measurements were made. In current-clamp configuration, increase in temperature from 22°C to 27°C induced a sustained but reversible hyperpolarization of the resting potential, suppressing the spontaneous firing. In contrast, cooling to 17°C depolarized membrane potential and induced spontaneous firing (Fig. 1A, B). Consistently, intracellular depolarizing current injection evoked neuronal firing, but the number of action potentials during the depolarization was temperature dependent. Furthermore, hyperpolarizing current injection revealed that an increase in temperature reduced the input resistance, whereas a decrease in

temperature increased it (R_{in} = 733 ± 63 MΩ at 17°C, 633 ± 25 MΩ at 22°C, and 585 ± 30 MΩ at 27°C; Fig. 1C). Similarly, action potential duration, measured at 0 mV, was markedly shortened from 17 ± 3.5 ms at 17°C to 7 ± 3.5 ms at 22°C and 5 ± 2.3 ms at 27°C. The previous observations: membrane hyperpolarization, reduction in input resistance, and shortening of action potential duration in response to increasing temperature suggested that an increase in a background potassium leak conductance may contribute to the temperature-dependent changes in the intrinsic electrical properties of XO neurons.

To test this possibility, membrane currents were subsequently recorded under symmetrical K^+ conditions. In voltage-clamp mode, square-pulse I–V curves showed a significant increase in leak conductance with warming under symmetrical K^+ conditions. Linear regression estimated a leak conductance of 12.26 nS at 17°C, 23.77 nS at 22°C, and 39.46 nS at 27°C (n = 10), supporting the idea that background K^+ conductance is suppressed at lower temperatures and enhanced at higher temperatures (Fig. 1D). At -60 mV, mean current amplitude was − 0.60 ± 0.12 nA at 17°C, -1.18 ± 0.18 nA at 22°C, and − 2.10 ± 0.26 nA at 27°C, corresponding to a 3.5 fold increase. At + 60 mV, currents increased from 0.86 ± 0.12 nA at 17°C to 2.56 ± 0.47 nA at 27°C a 3-fold increase. One-way ANOVA revealed significant effects of temperature ($F(2.27) = 14.13$, $p < 0.0001$ at − 60 mV; $F(2.27) = 6.06$, $p < 0.0067$ at + 60 mV), and Tukey's post hoc tests confirmed significant differences between 17 vs. 27°C ($p < 0.0001$) and 22 vs. 27°C ($p = 0.0088$) at − 60 mV and 17 vs. 27°C ($p = 0.0047$) at + 60 mV. To quantify temperature sensitivity and highlight the increase in Q10, currents were normalized to their amplitudes at 17°C (Fig. 1E). At the single-channel level (cell-attached), in symmetrical K^+ solutions, channel open probability (P_o) at 50 mV also displayed strong temperature dependence (one-way ANOVA, $F(2.27) = 9.512$, $p < 0.0007$; Tukey post hoc, $p < 0.0001$). Mean P_o increased from 0.056 ± 0.045 at 17°C to 0.66 ± 0.055 at 22°C and 0.79 ± 0.097 at 27°C, reflecting a Q_{10} of 14.1 from 17 to 27°C. These results indicate that the macroscopic thermosensitive current in X-organ neurons arises from an increase in channel activity (open probability), with asymmetric voltage dependence of thermal sensitivity (Fig. 1F, G). Together, these findings revealed that warming enhances a background leak conductance through an increase in single-channel activity, providing explanation for the temperature-dependent changes in the electrical properties of XO neuron. Because these properties closely resemble those of thermosensitive K_{2P} channels, we next searched the *P. clarkii* transcriptome for candidate K_{2P} channel sequences.

Identification and bioinformatics analysis of a novel K_{2P} subunit from P. clarkii

To identify the putative subunit responsible for the temperature-dependent potassium leak conductance, we used as probes sequences for K_{2P} channels from other organisms. We detected Pc_6896, a transcribed RNA sequence with similarities to mammalian K_{2P} subunits in the Procambarus Transcriptomes Shotgun Assembly (TSA) (Manfrin et al., 2015; Tom et al., 2014). We detected in the *Procambarus* Transcriptomes Shotgun Assembly (TSA) (Manfrin et al., 2015; Tom et al., 2014) Pc_6896, whose translated sequence shows similarities to mammalian K_{2P} subunits. This sequence was named $PcK_{2P}1$ (accession number: PX922273). Its open reading frame (1,254 bp) encodes a predicted protein of 417 amino acids. This sequence was amplified and cloned using RT-PCR and total RNA isolated from

P. clarkii eyestalk. Variant confirmation and full-length open reading frame sequencing of $PcK_{2P}1$ were carried out using the Sanger method. The amino acid sequence of $PcK_{2P}1$ was analyzed using the BLASTP algorithm against the protein database to identify the protein family to which it belongs. The results showed that all significant alignments were with K_{2P} channels subunits. Additionally, features of K_{2P} channels were found, such as the canonical topology with two selectivity filter motifs, four transmembrane helices, a large extracellular loop between TM1 and TM2, and short and long N- and C-terminal domains, respectively (Fig. 2A, B). Through bioinformatic analysis, we identified four hydrophobic transmembrane domains: TM1 (V7–L27), TM2 (I147–S167), TM3 (A199–T219), and TM4 (I260–I280) (Fig. 2C). TM1 and TM2 are connected by a 120-residue segment that includes the first pore helix, the first selectivity filter motif, and an extracellular loop containing two α-helices that likely form the cap domain (T44–W68). We also found multiple sites linked to post-translational modifications. The amino acid sequence contains 37 potential phosphorylation sites: 23 on Ser, 10 on Thr, and 4 on Tyr residues (Fig. 2D). Sequence has three predicted N-linked glycosylation sites and three O-linked glycosylation sites (Fig. 2E, F). Primary subcellular localization analysis indicates that $PcK_{2P}1$ is anchored in the plasma membrane (confidence score = 0.6868) and is likely to act as a transmembrane protein (confidence score = 0.9880).

Finally, the three-dimensional structure was predicted using SWISS-MODEL with the human TREK-2 channel (PDB 4XDL) selected as the structural template. The template showed 33.07% sequence identity and 62% coverage with PcK2P1, and the predicted model was consistent with a homodimeric assembly (QSQE = 0.69). Although the model exhibited moderate overall confidence (QMEANDisCo = 0.52) and covered residues 2–288, the sequence alignment revealed conservation of the threonine residues associated with the K^+ selectivity filter of TREK-2. These conserved residues were positioned within the predicted pore region, in a spatial arrangement corresponding to the K^+ coordination site observed in the template. (Fig. 2G). Altogether, these findings support the idea that $PcK_{2P}1$ sequence has the potential to form a functional K_{2P} channel, exhibiting the structural features characteristic of this family.

Sequence and phylogenetic analysis

To explore the relationship between $PcK_{2P}1$ and other K_{2P} channels, we performed a multiple sequence alignment focusing on the two pore helices and the selectivity filter motifs from both vertebrate and invertebrate K_{2P} sequences. The alignment revealed that these regions are highly conserved, especially the selectivity filter motifs, which are highly conserved among all K_{2P} family members (Fig. 3A). To further assess sequence similarity, we generated a pairwise identity matrix based on the alignment. $PcK_{2P}1$ showed the highest identity with human TREK-2 (29.23%) and *Aplysia californica* AcK2p2 (26.44%) (Fig. 3B). A phylogenetic tree was then constructed using representative K_{2P} sequences from various species. $PcK_{2P}1$ clustered within the invertebrate group, closely associated with *Caenorhabditis elegans* TWK-18, *Drosophila melanogaster* ORK-1, and *A. californica* AcK2p2 (Fig. 3C). Although the sequence identity between $PcK_{2P}1$ and other K_{2P} channels is relatively low, its conserved structural

elements clearly classify it as a member of the K_{2P} family. These findings suggest that $PcK_{2P}1$ may represent a *P. clarkii*-specific or crustacean-specific K_{2P} channel type.

Figure 3. Sequence and phylogenetic analysis of the PcK $_{2P}$ 1 subunit. A. Alignment of $PcK_{2P}1$ regions. Potassium selectivity filter motifs (P1 and P2, red boxes) and pore helices (PH1 and PH2, gray line) from $PcK_{2P}1$ and other K_{2P} channel subunits; $PcK_{2P}1$ is highlighted in red letters. P1 and P2 show high sequence identity within both vertebrate and invertebrate K_{2P} members, including C. elegans TWK-18 (Q18120), *Aplysia californica* AcK2p1 (AAN62847.1) and AcK2p2 (DQ166529.1), as well as human TRAAK (Q9NYG8), TREK-1 (O95069), and TREK-2 (P57789). Identical and similar residues are highlighted in black and gray, respectively. **B.** Pairwise identity matrix showing sequence similarity between $PcK_{2P}1$ and selected K_{2P} subunits. Each box displays the percentage of shared identity between subunits. **C**. Phylogenetic tree showing the evolutionary relationships of $PcK_{2P}1$ with other K_{2P} channels. The tree was inferred using the Maximum Likelihood method and the JTT matrix-based model. $PcK_{2P}1$ (red circle) clusters with invertebrate K_{2P} subunits and is part of a branch closely related to the human TREK subfamily.

Functional expression of PcK1 in HEK293T cells

HEK293T cells were transfected with the $PcK_{2P}1$ cDNA to investigate whether it forms a functional channel. Whole-cell and cell-attached patch-clamp recordings were performed using symmetrical K^+ solutions in the bath. As expected, $PcK_{2P}1$ formed a functional channel. Transfected HEK293T cells displayed significantly larger currents than non-transfected cells in response to a voltage ramp from − 140 to + 60 mV over 1 s. Linear regression estimated leak conductance of control cells was 24.42 pS, and in transfected cells the conductance increased to 78.64 pS (Fig. 4A). Current densities increased from − 9.52 ± 0.81 pA/pF in control cells to − 45.41 ± 3.11 pA/pF in transfected cells at − 60 mV and 23.37 ± 3.08 pA/pF in control cells to 65.98 ± 6.44 pA/pF in transfected cells at + 60 mV (unpaired t−test with Welch's correction, $p < 0.0001$; Fig. 4B). These results indicate that $PcK_{2P}1$-expressing cells exhibit a K^+ leak current with outward rectification.

The reversal potential (E_{rev}) shifted to more positive values as extracellular [K^+] increased, consistent with the change in the established E_{K+}, strongly suggesting selective permeability to K^+. Mean E_{rev} values were 0.1 ± 0.62 mV at 145 mM K^+, − 7.61 ± 0.13 mV at 110 mM K^+, − 28.6 ± 2.45 mV at 40 mM K^+, and − 72.03 ± 2.16 mV at 5 mM K^+ (Fig. 4C). One-way ANOVA revealed a significant effect of extracellular [K^+] on E_{rev} ($p < 0.0001$). Tukey's post hoc test confirmed that all pairwise comparisons were significant ($p < 0.0001$ for each). Linear regression of E_{rev} as a function of log[K^+] yielded a slope of 49.9 mV per decade, indicating a dependence on extracellular potassium (Fig. 4D), although lower than the theoretical Nernst prediction for a perfectly selective K^+ channel (~ 58 mV/decade at room temperature).

Having established that $PcK_{2P}1$ forms a functional potassium-permeable channel with distinct macroscopic properties, we characterized its single-channel behavior in cell-attached patches in transfected HEK293T cells under symmetrical K^+ conditions. No $PcK_{2P}1$ activity was detected in patches from untransfected cells (data not shown). Representative recordings (Fig. 5A) revealed robust channel activity at both + 80 and − 80 mV, with frequent flickering and prolonged bursts of opening. Two distinct conductance states were consistently observed within the same patch, corresponding to small (S) and large (L) conductance states (Fig. 5B), suggesting the presence of sub-conductance states. The large- and small-conductance states exhibited conductances of 106.6 ± 0.45 and 40.86 ± 0.52 pS, respectively (Fig. 5C, D). $PcK_{2P}1$ channels displayed higher voltage-dependent open probability (P_o) at hyperpolarized potentials. P_o values were 0.47 ± 0.08 at − 80 mV compared with 0.24 ± 0.06 at + 80 mV (Fig. 5E). Dwell-time histograms revealed a predominantly short-opening state with occasional longer events (Fig. 5F), resulting in mean opening times of 4.11 ± 0.45 ms at − 80 mV and 3.42 ± 0.49 ms at + 80 mV (Fig. 5G).

The PcK1 channel is thermosensitive

Once we demonstrated that $PcK_{2P}1$ forms a functional K^+ channel with distinct single-channel properties, we next examined whether its activity is influenced by temperature, based on the thermal preference of *P. clarkii*. Whole-cell currents were recorded at 20, 25, and 30°C using voltage-ramp protocols from − 140 to + 60 mV (holding potential 0 mV). As shown in Fig. 6A, $PcK_{2P}1$ currents were small at 20°C, modestly increased at 25°C, and became large and with a slightly more pronounced outward rectifying at 30°C. At − 60 mV, current amplitude was temperature dependent (Fig. 6B). One-way ANOVA shows a significant main effect of temperature ($F(2,39) = 22.81$, $p < 0.0001$). Post hoc Tukey's tests confirmed significant differences between all conditions (20 vs. 25°C: $p = 0.0016$; 20 vs. 30°C: $p < 0.0001$; 25 vs. 30°C: $p < 0.0001$). Mean currents were − 33.75 ± 2.80 pA at 20°C, − 42.89 ± 4.13 pA at 25°C, and − 82.12 ± 7.87 pA at 30°C. At + 60 mV, currents also increased significantly with temperature. One-way ANOVA indicated a significant effect ($F(2,39) = 16.63$, $p < 0.0001$), and Tukey's multiple comparisons showed strong differences between all pairs (20 vs. 25°C: $p < 0.0001$; 20 vs. 30°C: $p < 0.0001$; 25 vs. 30°C: $p = 0.0005$). Average currents were 55.36 ± 6.24 pA at 20°C, 74.37 ± 6.37 pA at 25°C, and 134.00 ± 14.97 pA at 30°C. To further assess temperature sensitivity, current amplitudes were normalized to their values at 20°C and expressed as fold increase (Fig. 6C). Between 20 and 30°C, currents increased approximately 2.4-fold at both voltages (−60 mV: 2.43; +60 mV: 2.42). The corresponding Q_{10} values were 2.40 (−60 mV) and 2.42 (+ 60 mV), indicating a steep temperature dependence consistent with values reported for thermosensitive ion channels (Lamas et al., 2019).

We next assessed whether the single-channel properties of $PcK_{2P}1$ are modulated by temperature in the cell-attached configuration. Representative traces at − 80 and + 80 mV show that channel activity increased with rising temperature, displaying more frequent openings and longer bursts at 30°C (Fig. 6D). Data were obtained from ~ 10 s of current recording per temperature and analyzed as described previously. Dwell-time histograms fitted with single-exponential functions revealed that the mean open time was not significantly affected by temperature (Fig. 6E, F). At − 80 mV, the mean open

time was 4.62 ± 1.06 ms at 20°C, 5.39 ± 0.82 ms at 25°C, and 4.52 ± 0.24 ms at 30°C (one-way ANOVA, $F(2,29) = 0.3651$, $p = 0.697$; Tukey's test, n.s.). Similarly, at + 80 mV, mean open times were 6.77 ± 1.11 ms, 4.96 ± 1.19 ms, and 6.19 ± 0.35 ms at 20, 25, and 30°C, respectively (ANOVA, $F(2,29) = 0.9245$, $p = 0.41$; Tukey's test, n.s.). In contrast, open probability (P_o) of $PcK_{2P}1$ was profoundly modulated by temperature (Fig. 6G). At − 80 mV, P_o increased with Q_{10} of 3.3 from 0.16 ± 0.02 at 20°C to 0.33 ± 0.02 at 25°C, and to 0.53 ± 0.01 at 30°C (ANOVA, $F(2,29) = 119.1$, $p < 0.0001$; Tukey: all pairwise comparisons, $p < 0.0001$). At + 80 mV, P_o was increased with Q_{10} of 3.6 from 0.20 ± 0.02 at 20°C, 0.16 ± 0.02 at 25°C, and 0.73 ± 0.01 at 30°C (ANOVA, $F(2,29) = 324.9$, $p < 0.0001$). Tukey's test showed no difference between 20°C and 25°C (p = n.s.), but highly significant increases at 30°C versus both lower temperatures ($p < 0.0001$). Taken together, these results demonstrate that although the mean opening time of $PcK_{2P}1$ is temperature-insensitive, P_o increase sharply at higher temperature, showing that channel gating underlies the thermal sensitivity of $PcK_{2P}1$, indicating that warming increased $PcK_{2P}1$ channel activity without a detectable change in mean open time.

Modulation of $PcK_{2P}1$ in HEK293T cells

To evaluate whether $PcK_{2P}1$ behaves as a stimulus integrator, like other K_{2P} channels (Enyedi and Czirják, 2010), we examined its response to different modulators and drugs. All recordings, except mechanical pressure, were performed in symmetrical 145 mM K^+ solution using a voltage ramp protocol from − 100 to + 60 mV in the presence or absence of the modulator in HEK293T cells expressing $PcK_{2P}1$ (Fig. 7). First, we tested whether Mg^{2+} blocks $PcK_{2P}1$ as described for other K_{2P} channels (Maingret et al., 2002). At both − 60 mV and + 60 mV, data distributions passed the Shapiro–Wilk normality test, so paired t-tests were used. Mg^{2+} (3 mM) significantly decreased current amplitude at both voltages ($p = 0.0006$). At − 60 mV, mean currents were − 22.67 ± 2.99 pA with Mg^{2+} and − 41.45 ± 4.57 pA without Mg^{2+}. At + 60 mV, currents were 43.75 ± 5.96 pA with Mg^{2+} and 57.13 ± 5.37 pA without Mg^{2+} (n = 13; Fig. 7A). Next, we tested the effect of 10 µM arachidonic acid (AA, Patel et al., 1998; Fig. 7B). At − 60 mV, data passed the normality test, and paired t-tests showed a significant increase in current due to AA ($p = 0.0151$). This effect was confirmed by a Wilcoxon signed-rank test ($p = 0.0313$). The mean currents were − 114.6 ± 23.8 pA with AA and − 29.86 ± 1.91 pA in control cells. At + 60 mV, control values failed the normality test, so the Wilcoxon test was used, also showing a significant increase in current amplitude ($p = 0.0313$). Mean currents were 128.5 ± 20.7 pA with AA and 45.46 ± 6.91 pA in control (n = 6). To examine $PcK_{2P}1$ channel activity under atmospheric pressure (control) and during sustained membrane stretch (− 100 mmHg) in the cell-attached configuration with symmetrical K^+. Channel activity was strongly enhanced at both − 80 mV and + 80 mV when negative pressure was applied to the patch (Fig. 7C). At − 80 mV, NP_o increased from 0.31 ± 0.029 to 2.02 ± 0.076 (6.4-fold), and at + 80 mV it increased from 0.23 ± 0.022 to 1.55 ± 0.077 (6.5-fold) (Fig. 7D). Each condition was analyzed from ~ 20 s of current recording. An unpaired t-test with Welch's correction confirmed a significant increase in activity at both − 80 mV ($p = 0.0001$) and + 80 mV ($p = 0.0001$).

Finally, because K_{2P} channels are typically resistant to classical K^+ channel blockers due to their pore architecture, we assessed $PcK_{2P}1$ sensitivity to tetraethylammonium (TEA, 10 mM). At − 60 mV and + 60 mV, data were normally distributed, and paired t-tests were applied. At − 60 mV, TEA produced no significant inhibition (p = 0.2652), with mean currents of − 33.57 ± 4.72 pA in TEA and − 36.33 ± 5.44 pA in control cells. At + 60 mV, however, TEA caused a small but significant reduction in macroscopic current (p = 0.0428), with currents of 48.34 ± 6.11 pA in TEA and 61.98 ± 4.21 pA in control cells (n = 8; Fig. 7E). In contrast, we tested another quaternary ammonium (QA) ion, tetrahexylammonium (THexA, 10 µM). Data at − 60 mV and + 60 mV were also normally distributed, and paired t-tests were used. At − 60 mV, THexA produced a robust inhibition (p = 0.0013), reducing mean currents from − 31.36 ± 1.69 pA in control cells to − 16.15 ± 2.79 pA in THexA. At + 60 mV, THexA also significantly inhibited $PcK_{2P}1$ currents (p = 0.0003), with currents of 19.38 ± 2.72 pA in THexA and 63.36 ± 6.25 pA in control cells (n = 8; Fig. 7F).

Differential expression and FISH of PcK $_{2P}$ 1 in eyestalk of P. clarkii

To investigate the expression pattern of $PcK_{2P}1$ in *P. clarkii* eyestalk and other regions, we performed RT-PCR amplifications on different neural and abdominal tissues. A clear band of the expected size (1,048 bp) was detected in all tissues examined (XO, medulla terminalis, medulla interna, medulla externa abdominal ganglia and muscle tissue; Fig. 8A). GAPDH was consistently amplified in all samples and was used as expression control. This nervous system expression is consistent with our electrophysiological findings and suggests a putative role of $PcK_{2P}1$ in regulating neuronal excitability.

To further assess $PcK_{2P}1$ expression at the cellular level, we performed fluorescent *in situ* hybridization (FISH) using a digoxigenin (DIG)-labeled antisense riboprobe. Strong hybridization signal was detected in neurons of the X-organ (XO) within the eyestalk, confirming the presence of $PcK_{2P}1$ mRNA in these cells (Fig. 8B). The sense probe used as a negative control showed no signal (Fig. 8C), validating label specificity. The detection of $PcK_{2P}1$ transcripts in XO neurons reinforces its functional presence and potential contribution to excitability in these neurosecretory cells.

Discussion

In this study, we report $PcK_{2P}1$, a novel invertebrate K_{2P} channel identified in the neurosecretory system of *P. clarkii*. This channel exhibits topological and electrophysiological properties reminiscent of mammalian TREK channels, while also displaying unique characteristics that suggest a potential role as a multimodal stimulus integrator within this neurosecretory system.

Electrophysiological recordings show that warming increases background K^+ conductance in X-organ neurons, consistent with a mechanism proposed for mammalian dorsal root and trigeminal thermoreceptive neurons (Talley et al., 2003). In these systems, increased K_{2P}-mediated leak promotes hyperpolarization and limits excitability, whereas reduced leak favors depolarization and firing (Goldstein et al., 2001; Enyedi and Czirják, 2010; Renigunta et al., 2015)

Although macroscopic currents displayed outward rectification, as reported for TREK-1 (Maingret et al., 2000), relative thermal sensitivity was greater at hyperpolarized potentials. This behavior may reflect temperature-dependent changes in channel gating, although changes in unitary conductance cannot be excluded. Together, these findings support the presence of a thermosensitive K^+ leak current in X-organ neurons, consistent with the participation of K_{2P} channels.

Despite modest amino acid identity with mammalian TREK-1 and TREK-2 and invertebrate channels such as *Aplysia* AcK2P2 (Jezzini et al., 2006), $PcK_{2P}1$ preserves the canonical 4TM/2P K_{2P} architecture (Enyedi and Czirják, 2010). Structural predictions further suggest a homodimeric organization with four pore domains, similar to human TWIK-1 (Miller and Long., 2012) and TRAAK (Brohawn et al., 2012).

$PcK_{2P}1$ contains an extended TM1–P1 extracellular linker predicted to form extracellular cap characteristic of K_{2P} channels, a structure implicated in mammalian channel assembly, gating, and pharmacology (Clarke et al., 2008; Miller and Long, 2012; Vivier et al., 2016). Its P1 and P2 selectivity filter sequences also show slight asymmetry, consistent with a proposed model in which filter flexibility supports polymodal gating while preserving K^+ permeation (Bagriantsev et al., 2011; Piechotta et al., 2011; Schewe et al., 2016). These structural features suggest conserved functional roles in $PcK_{2P}1$.

$PcK_{2P}1$ expression in HEK293T cells produced an outwardly rectifying K^+ current that persisted under symmetrical K^+ conditions and did not conform to Goldman–Hodgkin–Katz predictions, as reported for TREK-1 and TREK-2 (Fink et al., 1996; Lesage et al., 2000). Ion substitution experiments supported high K^+ selectivity, with reversal potential shifts approaching the Nernst prediction, like TASK-3 and TRAAK (Kim et al., 2000; Fink et al., 1998).

Single-channel recordings revealed small- and large-conductance states in $PcK_{2P}1$. Similar heterogeneity in TREK-1 and TREK-2 has been associated with alternative translation initiation (ATI) and intracellular signaling, with individual ATI isoforms also displaying distinct conductance levels (Li et al., 2006; Kang et al., 2007; Thomas et al., 2008; Simkin et al., 2008). A possible explanation for this behavior is that multiple N-terminal methionine residues and putative phosphorylation sites in $PcK_{2P}1$ suggest that analogous mechanisms may contribute to its conductance diversity, although neither ATI nor phosphorylation-dependent modulation has been demonstrated.

$PcK_{2P}1$ showed weak voltage dependence at the single-channel level, with more activity at hyperpolarized potentials, yet displayed macroscopic outward rectification. This behavior may involve both intrinsic voltage-dependent gating (Schewe et al., 2016) and voltage-dependent Mg^{2+} block, as reported for TREK-1 (Maingret et al., 2002; Bockenhauer et al., 2001). Extracellular Mg^{2+} removal partially linearized the current–voltage relationship, supporting a contribution of Mg^{2+} to the observed rectification.

$PcK_{2P}1$ exhibited robust thermosensitivity; warming increased leak current and channel open probability (P_O) without significantly changing mean open time, with Q_{10} values comparable to those of mammalian

TREK channels (Maingret et al., 2000; Kang et al., 2005; Lamas et al., 2019). These findings support temperature-dependent modulation of PcK2P1 gating, although kinetic differences from TREK-2 and TRAAK may reflect distinct underlying mechanisms (Schneider et al., 2014). Such functional divergence is consistent with species-dependent variation in K_{2P} thermosensitivity associated with differences in the C-terminal domain (Kang et al., 2005; Cordeiro and Musinszki, 2025). TREK-1 thermosensitivity requires cytoskeletal interactions and PKA-dependent phosphorylation within a C-terminal temperature-responsive element (TRE) (Cordeiro and Musinszki, 2025). $PcK_{2P}1$ contains a region with similar positive charge and a putative PKA phosphorylation site but lacks the residues required for MAP2 binding in TREK-1. These features suggest that $PcK_{2P}1$ may retain thermosensitivity through partially distinct molecular interactions.

Beyond temperature, K_{2P} channels are known for being polymodal ion channels. $PcK_{2P}1$ responds to arachidonic acid and mechanical stimulation, characteristic properties of the TREK subfamily (Maingret, et al., 2000; Meadows et al., 2000 and Lesage et al., 2000). Both stimuli increased channel activity, consistent with lipid bilayer–mediated gating mechanisms described for mechanosensitive K_{2P} channels (Patel et al., 2001; Lotshaw, 2007). $PcK_{2P}1$ contains clusters of charged residues within its C-terminal domain that may mediate interactions with membrane lipids, analogous to mechanisms described for TRAAK channels (Patel et al., 1998; Brohawn et al., 2014).

Pharmacological analysis further supports classification of $PcK_{2P}1$ as a canonical K_{2P} channel. $PcK_{2P}1$ was insensitive to tetraethylammonium but inhibited by longer-chain quaternary ammonium ions such as tetrahexylammonium, consistent with the presence of an extracellular cap domain positioned directly above the selectivity filter that restricts access to the pore (Piechotta et al., 2011; Braun, 2012; Concha et al., 2018).

$PcK_{2P}1$ expression in X-organ neurons, demonstrated by fluorescence in situ hybridization, provides a physiological context for its polymodal properties. Its sensitivity to temperature, mechanical forces, and lipid modulators suggests a role in adjusting neuronal excitability and neurosecretory output to changing environmental conditions (García and Aréchiga, 1998). This proposed role is consistent with the regulation of neuronal excitability by mammalian TREK-1, TRAAK, TASK-1, and TASK-3 channels (Maingret et al., 2000; Musset et al., 2006; Noël et al., 2009).

The identification of $PcK_{2P}1$ expression in X-organ neurons highlights a conserved functional role for K_{2P} channels despite significant sequence divergence between $PcK_{2P}1$ and mammalian TREK channels (Enyedi and Czirják, 2010). This interpretation is consistent with the deep evolutionary origin of the six K_{2P} channel subfamilies (Park et al., 2024).

Taking together, our findings identify $PcK_{2P}1$ as a polymodal, thermosensitive K_{2P} channel in an invertebrate neuroendocrine system. These results extend our understanding of thermosensitive K_{2P} channel described in an invertebrate species and highlights an evolutionarily conserved role for

polymodal leak channels in coupling environmental sensing to neuronal output. These results extend the functional repertoire of K_{2P} channels beyond vertebrate systems and provide new insight into the molecular mechanisms underlying sensory integration in invertebrate neuroendocrine networks.

Declarations

Conflict of interest statement

The authors declare no competing financial interests.

Author Contribution

J.M.H.M.: Conceptualization; data curation; formal analysis; funding acquisition; investigation; methodology; validation; visualization; writing original draft. I.U.V.H., I.S.M.R and K.Y.M.V: Investigation; methodology. E.S.J.: Investigation; methodology; resources. J.M.A.: Conceptualization; data curation; formal analysis; funding acquisition; resources; supervision. U.G.H: Conceptualization; formal analysis; funding acquisition; investigation; resources; supervision.

Acknowledgement

Juan Manuel Hernández-Martínez was supported by Consejo Nacional de Ciencia y Tecnología (CONACyT), México (Scholarship number: 859060).This research was supported by Dirección General de Asuntos del Personal Académico of the Universidad Nacional Autónoma de México (DGAPA – UNAM), Grant number: IN220524 to J.M.A.The authors would like to thank Alejandro Cruz Monsalvo-Reyes for his support with sequencing, Rosana Sofía Fiorentino Pérez and Francisco Javier de los Santos for their assistance with cell culture.María A. Cabañas-Cortés provided technical support in capturing confocal microscopy images at the Confocal Microscopy Unit at the Cell Biology Department of CINVESTAV-IPN.

Data Availability

The PcK2P1 nucleotide sequence is available in GenBank under accession number PX922273.

References

1. Bagriantsev SN, Peyronnet R, Clark KA, Honoré E, Minor DL Jr (2011) Multiple modalities converge on a common gate to control K2P channel function. EMBO J 30:3594–3606. https://doi.org/10.1038/emboj.2011.230
2. Bagriantsev SN, Clark KA, Minor DL Jr (2012) Metabolic and thermal stimuli control K2P2.1 (TREK-1) through modular sensory and gating domains. EMBO J 31:3297–3308.

https://doi.org/10.1038/emboj.2012.171

3. Ben Soussia I, El Mouridi S, Kang D, Leclercq-Blondel A, Khoubza L, Tardy P, Zariohi N, Gendrel M, Lesage F, Kim EJ, Bichet D, Andrini O, Boulin T (2019) Mutation of a single residue promotes gating of vertebrate and invertebrate two-pore domain potassium channels. Nat Commun 10:787. https://doi.org/10.1038/s41467-019-08710-3
4. Blom N, Gammeltoft S, Brunak S (1999) Sequence-and structure-based prediction of eukaryotic protein phosphorylation sites. J Mol Biol 294:1351–1362. https://doi.org/10.1006/jmbi.1999.3310
5. Bockenhauer D, Zilberberg N, Goldstein SAN (2001) KCNK2: reversible conversion of a hippocampal potassium leak into a voltage-dependent channel. Nat Neurosci 4:486–491. https://doi.org/10.1038/87434
6. Boulant JA (1998) Cellular mechanisms of temperature sensitivity in hypothalamic neurons. In: Brain function in hot environment (Sharma HS, Westman J, eds), Prog Brain Res 115:3–8. https://doi.org/10.1016/S0079-6123(08)62026-9
7. Brauchi S, Orio P, Latorre R (2004) Clues to understanding cold sensation: thermodynamics and electrophysiological analysis of the cold receptor TRPM8. Proc Natl Acad Sci U S A 101:15494–15499. https://doi.org/10.1073/pnas.0406773101
8. Braun AP (2012) Two-pore domain potassium channels: variation on a structural theme. Channels 6:139–140. https://doi.org/10.4161/chan.20973
9. Brohawn SG, del Mármol J, MacKinnon R (2012) Crystal structure of the human K2P TRAAK, a lipid- and mechano-sensitive K + ion channel. Science 335:436–441. https://doi.org/10.1126/science.1213808
10. Brohawn SG, Campbell EB, MacKinnon R (2014) Physical mechanism for gating and mechanosensitivity of the human TRAAK K+ channel. Nature 516:126–130. https://doi.org/10.1038/nature14013
11. Chemin J, Patel AJ, Duprat F, Lauritzen I, Lazdunski M, Honoré E (2005) A phospholipid sensor controls mechanogating of the K+ channel TREK-1. EMBO J 24:44–53. https://doi.org/10.1038/sj.emboj.7600494
12. Chemin J, Patel AJ, Duprat F, Sachs F, Lazdunski M, Honoré E (2007) Up-and down-regulation of the mechano-gated K2P channel TREK-1 by PIP2. Pflugers Arch 455:97–103. https://doi.org/10.1007/s00424-007-0250-2
13. Chung JS, Zmora N (2008) Functional studies of crustacean hyperglycemic hormones (CHHs) of the blue crab, Callinectes sapidus – the expression and release of CHH in eyestalk and pericardial organ in response to environmental stress. FEBS J 275:693–704. https://doi.org/10.1111/j.1742-4658.2007.06231.x
14. Chung JS, Zmora N, Katayama H, Tsutsui N (2010) Crustacean hyperglycemic hormone (CHH) neuropeptides family: functions, titer, and binding to target tissues. Gen Comp Endocrinol 166:447–454. https://doi.org/10.1016/j.ygcen.2009.12.011

15. Clarke CE, Veale EL, Wyse K, Vandenberg JI, Mathie A (2008) The M1P1 loop of TASK3 K2P channels apposes the selectivity filter and influences channel function. J Biol Chem 283:16946–16952. https://doi.org/10.1074/jbc.M801368200
16. Coetzee WA, Amarillo Y, Chiu J, Chow A (1999) Molecular diversity of K+ channels. Ann N Y Acad Sci 868:233–285. https://doi.org/10.1111/j.1749-6632.1999.tb11293.x
17. Cohen A, Ben-Abu Y, Hen S, Zilberberg N (2008) A novel mechanism for human K2P2.1 channel gating: facilitation of C-type gating by protonation of extracellular histidine residues. J Biol Chem 283:19448–19455. https://doi.org/10.1074/jbc.M801273200
18. Concha G, Bustos D, Zúñiga R, Catalán MA, Zúñiga L (2018) The insensitivity of TASK-3 K2P channels to external tetraethylammonium (TEA) partially depends on the cap structure. Int J Mol Sci 19:2437. https://doi.org/10.3390/ijms19082437
19. Cordeiro S, Musinszki M (2025) Thermosensitivity of TREK K2P channels is controlled by a PKA switch and depends on the microtubular network. Pflugers Arch Eur J Physiol 477:953–966. https://doi.org/10.1007/s00424-025-03089-1
20. Davis MW, Jorgensen EM (2022) ApE, a plasmid editor: A freely available DNA manipulation and visualization program. Front Bioinform 2:1–15. https://doi.org/10.3389/fbinf.2022.818619
21. Dedman A, Sharif-Naeini R, Folgering J, Duprat F, Patel AJ, Honoré E (2009) The mechano-gated K2P channel TREK-1. Eur J Neurosci 38:293–303. https://doi.org/10.1007/s00249-008-0318-8
22. Enyedi P, Czirják G (2010) Molecular background of leak K+ currents: two-pore domain potassium channels. Physiol Rev 90:559–605. https://doi.org/10.1152/physrev.00029.2009
23. Fink M, Duprat F, Lesage F, Reyes R, Romey G, Heurteaux C, Lazdunski M (1996) Cloning, functional expression and brain localization of a novel unconventional outward rectifier K+ channel. EMBO J 15:6854–6862. https://doi.org/10.1002/j.1460-2075.1996.tb01077.x
24. Fink M, Lesage F, Duprat F, Heurteaux C, Reyes R, Fosset M, Lazdunski M (1998) A neuronal two P domain K+ channel stimulated by arachidonic acid and polyunsaturated fatty acids. EMBO J 17:3297–3308. https://doi.org/10.1093/emboj/17.12.3297
25. García U, Grumbacher-Reinert S, Bookman R, Reuter H (1990) Distribution of Na + and K+ currents in soma. axons and growth cones of leech Retzius neurones in
26. culture J Exp Biol 150:1–17. https://doi.org/10.1242/jeb.150.1.1
27. García U, Onetti C, Valdiosera R, Aréchiga H (1994) Excitatory action of gama-aminobutyric acid (GABA) on crustacean neurosecretory cells. Cell Mol Neurobiol 14:71–88. https://doi.org/10.1007/BF02088590
28. García U, Aréchiga H (1998) Regulation of crustacean neurosecretory cell activity. Cell Mol Neurobiol 18:81–99. https://doi.org/10.1023/A:1022527210808
29. Gillooly JF, Brown JH, West GB, Savage VM, Charnov EL (2001) Effects of size and temperature on metabolic rate. Science 293:2248–2251. https://doi.org/10.1126/science.1061967

30. Goldstein SAN, Price LA, Rosenthal DN, Pausch MH (1996) ORK1, a potassium-selective leak channel with two pore domains cloned from Drosophila melanogaster by expression in Saccharomyces cerevisiae. Proc Natl Acad Sci USA 93:13256–13261. https://doi.org/10.1073/pnas.93.23.13256
31. Goldstein SAN, Bockenhauer D, O'Kelly I, Zilberberg N (2001) Potassium leak channels and the KCNK family of two-P-domain subunits. Nat Rev Neurosci 2:175184. https://doi.org/10.1038/35058574
32. Green MR, Sambrook J (2012) Molecular cloning: a laboratory manual, Ed 4. Cold Spring Harbor Laboratory Press, Cold Spring Harbor, NY
33. Gupta R, Jung E, Gooley AA, Williams KL, Brunak S, Hansen J (1999) Scanning the available Dictyostelium discoideum proteome for O-linked GlcNAc glycosylation sites using neural networks. Glycobiology 9:1009–1022. https://doi.org/10.1093/glycob/9.10.1009
34. Gupta R, Brunak S (2002) Prediction of glycosylation across the human proteome and the correlation to protein function. Pac Symp Biocomput 310–322. https://doi.org/10.1142/9789812799623_0029
35. Hallgren J, Tsirigos KD, Pedersen MD, Almagro Armenteros JJ, Marcatili P, Nielsen H, Krogh A, Winther O (2022) DeepTMHMM predicts alpha and beta transmembrane proteins using deep neural networks. https://doi.org/10.1101/2022.04.08.487609. bioRxiv
36. Honoré E (2007) The neuronal background K2P channels: focus on TREK-1. Nat Rev Neurosci 8:251–261. https://doi.org/10.1038/nrn2117
37. Jezzini SH, Moroz LL (2004) Identification and distribution of a two-pore domain potassium channel in the CNS of *Aplysia californica*. Mol Brain Res 127:27–38. https://doi.org/10.1016/j.molbrainres.2004.05.007
38. Jezzini SH, Reagin S, Kohn AB, Moroz LL (2006) Molecular characterization and expression of a two-pore domain potassium channel in the CNS of *Aplysia californica*. Brain Res 1094:47–56. https://doi.org/10.1016/j.brainres.2006.03.122
39. Jiang H, Liu J, Huang Q, Yang D (2024) Effects of short-term temperature stress on metabolic and digestive enzyme activities of *Procambarus clarkii*. Isr J Aquacult Bamidgeh 76:286–293. https://doi.org/10.46989/001c.126179
40. Jiménez-Vázquez EN, Díaz-Velásquez CE, Uribe RM, Arias JM, García U (2016) Molecular cloning and expression of a GABA receptor subunit from the crayfish *Procambarus clarkii*. J Neurosci Res 94:190–203. https://doi.org/10.1002/jnr.23695
41. Jones DT, Taylor WR, Thornton JM (1992) The rapid generation of mutation data matrices from protein sequences. Bioinformatics 8:275–282. https://doi.org/10.1093/bioinformatics/8.3.275
42. Kang D, Choe C, Kim D (2005) Thermosensitivity of the two-pore domain K+ channels TREK-2 and TRAAK. J Physiol 564:103–116. https://doi.org/10.1113/jphysiol.2004.081059
43. Kang D, Choe C, Cavanaugh E, Kim D (2007) Properties of single two-pore domain TREK-2 channels expressed in mammalian cells. J Physiol 583:57–69. https://doi.org/10.1113/jphysiol.2007.136150

44. Ketchum KA, Joiner WJ, Sellers AJ, Kaczmarek LK, Goldstein SAN (1995) A new family of outwardly rectifying potassium channel proteins with two pore domains in tandem. Nature 376:690–695. https://doi.org/10.1038/376690a0
45. Kim Y, Bang H, Kim D (2000) TASK-3, a new member of the tandem pore K+ channel family. J Biol Chem 275:9340–9347. https://doi.org/10.1074/jbc.275.13.9340
46. Lamas JA, Rueda-Ruzafa L, Herrera-Pérez S (2019) Ion channels and thermosensitivity: TRP, TREK, or both? Int J Mol Sci 20:2371. https://doi.org/10.3390/ijms20102371
47. Lesage F, Terrenoire C, Romey G, Lazdunski M (2000) Human TREK2, a two-pore domain mechano-sensitive K+ channel with multiple regulations by polyunsaturated fatty acids, lysophospholipids, and Gs, Gi, and Gq protein-coupled receptors. J Biol Chem 275:28398–28405. https://doi.org/10.1074/jbc.M002822200
48. Li XT, Dyachenko V, Zuzarte M, Putzke C, Preisig-Müller R, Isenberg G, Daut J (2006) The stretch-activated potassium channel TREK-1 in rat cardiac ventricular muscle. Cardiovasc Res 69:86–97. https://doi.org/10.1016/j.cardiores.2005.08.018
49. Liu B, Song X, Bai S, Dong C (2022) Crayfish (*Procambarus clarkii*) TRPA1 is required for the defense against *Aeromonas hydrophila* infection under high temperature conditions and contributes to heat sensing. *Comparative Biochemistry and Physiology Part B: Biochemistry and Molecular Biology, 257*, Article 110654. https://doi.org/10.1016/j.cbpb.2021.110654
50. Lotshaw DP (2007) Biophysical, pharmacological, and functional characteristics of cloned and native mammalian two-pore domain K+ channels. Cell Biochem Biophys 47:209–256. https://doi.org/10.1007/s12013-007-0007-8
51. Luo L, Huang JH, Liu DL, Jiang SG, Zhou FL, Jiang S, Yang QB, Li YD, Li T, Tan LQ, Yang LS (2022) Comparative transcriptome analysis of differentially expressed genes and pathways in *Procambarus clarkii* (Louisiana crawfish) under acute temperature stress. Genomics 114:110415. https://doi.org/10.1016/j.ygeno.2022.110415
52. Maingret F, Lauritzen I, Patel AJ, Heurteaux C, Reyes R, Lesage F, Lazdunski M, Honoré E (2000) TREK-1 is a heat-activated background K+ channel. EMBO J 19:2483–2491. https://doi.org/10.1093/emboj/19.11.2483
53. Maingret F, Honoré E, Lazdunski M, Patel AJ (2002) Molecular basis of voltage-dependent gating of TREK-1, a mechano-sensitive K+ channel. Biochem Biophys Res Commun 292:339–346. https://doi.org/10.1006/bbrc.2002.6674
54. Manfrin C, Tom M, de Moro G, Gerdol M, Giulianini PG, Pallavicini A (2015) The eyestalk transcriptome of red swamp crayfish *Procambarus clarkii*. Gene 557:28–34. https://doi.org/10.1016/j.gene.2014.12.001
55. Meadows HJ, Benham CD, Cairns W, Gloger I, Jennings C, Medhurst AD, Murdock P, Chapman CG (2000) Cloning, localisation and functional expression of the human orthologue of the TREK-1 potassium channel. Pflugers Arch 439:714–722. https://doi.org/10.1007/s004249900235

56. Miller AN, Long SB (2012) Crystal structure of the human two-pore domain potassium channel K2P1. Science 335:432–436. https://doi.org/10.1126/science.1213274
57. Murbartián J, Lei Q, Sando JJ, Bayliss DA (2005) Sequential phosphorylation mediates receptor-and kinase-induced inhibition of TREK-1 background potassium channels. J Biol Chem 280:30175–30184. https://doi.org/10.1074/jbc.M503862200
58. Musset B, Meuth SG, Liu GX, Derst C, Wegner S, Pape HC, Budde T, Preisig-Müller R, Daut J (2006) Effects of divalent cations and spermine on the K+ channel TASK- 3 and on the outward current in thalamic neurons. J Physiol 572:639–657. https://doi.org/10.1113/jphysiol.2006.106898
59. Noël J, Zimmermann K, Busserolles J, Deval E, Alloui A, Diochot S, Guy N, Borsotto M, Reeh P, Eschalier A, Lazdunski M (2009) The mechano-activated K+ channels
60. TRAAK and TREK-1 control both warm and cold perception. EMBO J 28:1308–1318. https://doi.org/10.1038/emboj.2009.57
61. Ødum MT, Teufel F, Thumuluri V, Almagro Armenteros JJ, Johansen AR, Winther O, Nielsen H (2024) DeepLoc 2.1: multi-label membrane protein type prediction using protein language models. Nucleic Acids Res W265–W270 52(Web Server issue. https://doi.org/10.1093/nar/gkae237
62. Park SJ, Silic MR, Staab PL, Chen J, Zackschewski EL, Zhang G (2024) Evolution of two-pore domain potassium channels and their gene expression in zebrafish embryos. Dev Dyn 253:722–749. https://doi.org/10.1002/dvdy.690
63. Patel AJ, Honoré E, Maingret F, Lesage F, Fink M, Duprat F, Lazdunski M (1998) A mammalian two-pore domain mechano-gated S-like K+ channel. EMBO J 17:4283–4290. https://doi.org/10.1093/emboj/17.15.4283
64. Patel AJ, Lazdunski M, Honoré E (2001) Lipid and mechano-gated 2P domain K+ channels. Curr Opin Cell Biol 13:422–427. https://doi.org/10.1016/S0955-0674(00)00231-3
65. Payette AL, McGaw IJ (2003) Thermoregulatory behavior of the crayfish *Procambarus clarkii* in a burrow environment. Comp Biochem Physiol Mol Integr Physiol 136:539–556. https://doi.org/10.1016/S1095-6433(03)00203-4
66. Pérez-Polanco P, Garduño J, Cebada J, Zarco N, Segovia J, Lamas M, García U (2011) GABA and GAD expression in the X-organ sinus gland system of the *Procambarus clarkii* crayfish: inhibition mediated by GABA between X-organ neurons. J Comp Physiol A 197:923–938. https://doi.org/10.1007/s00359-011-0653-6
67. Piechotta PL, Rapedius M, Stansfeld PJ, Bollepalli MK, Erhlich G, Andres-Enguix I, Fritzenschaft H, Decher N, Sansom MSP, Tucker SJ, Baukrowitz T (2011) The pore structure and gating mechanism of K2P channels. EMBO J 30:3607–3619. https://doi.org/10.1038/emboj.2011.268
68. Renigunta V, Schlichthörl G, Daut J (2015) Much more than a leak: structure and function of K2P-channels. Pflugers Arch 467:867–894. https://doi.org/10.1007/s00424-015-1703-7
69. Sánchez-Jaramillo E, Wittmann G, Menyhért J, Singru P, Gómez-González GB, Sánchez-Islas E, Yáñez-Recendis N, Pimentel-Cabrera JA, León-Olea M, Gereben B, Fekete C, Charli JL, Lechan RM

(2022) Origin of thyrotropin-releasing hormone neurons that innervate the tuberomammillary nuclei. Brain Struct Funct 227:2329–2347. https://doi.org/10.1007/s00429-022-02527-5

70. Sandoz G, Douguet D, Chatelain F, Lazdunski M, Lesage F (2009) Extracellular acidification exerts opposite actions on TREK-1 and TREK-2 potassium channels via a single conserved histidine residue. Proc Natl Acad Sci U S A 106:14628–14633. https://doi.org/10.1073/pnas.0906267106
71. Schewe M, Nematian-Ardestani E, Sun H, Musinszki M, Cordeiro S, Bucci G, de Groot BL, Tucker SJ, Rapedius M, Baukrowitz T (2016) A non-canonical voltage-sensing mechanism controls gating in K2P K+ channels. Cell 164:937–949. https://doi.org/10.1016/j.cell.2016.02.002
72. Schneider ER, Anderson EO, Gracheva EO, Bagriantsev SN (2014) Temperature sensitivity of two-pore (K2P) potassium channels. In: Latorre R (ed) Current topics in membranes, vol 74. Academic, New York, pp 113–133. https://doi.org/10.1016/B978-0-12-800181-3.00005-1
73. Simkin D, Cavanaugh EJ, Kim D (2008) Control of the single-channel conductance of K2P10.1 (TREK-2) by the amino terminus: role of alternative translation initiation. J Physiol 586:5651–5663. https://doi.org/10.1113/jphysiol.2008.161927
74. Talley EM, Sirois JE, Lei Q, Bayliss DA (2003) Two-pore-domain (KCNK) potassium channels: dynamic roles in neuronal function. Neuroscientist 9:46–56. https://doi.org/10.1177/1073858402239590
75. Thomas D, Plant LD, Wilkens CM, McCrossan ZA, Goldstein SAN (2008) Alternative translation initiation in rat brain yields K2P2.1 potassium channels permeable to sodium. Neuron 58:859–870. https://doi.org/10.1016/j.neuron.2008.04.016
76. Tom M, Manfrin C, Chung SJ, Sagi A, Gerdol M, de Moro G, Pallavicini A, Giulianini PG (2014) Expression of cytoskeletal and molt-related genes is temporally scheduled in the hypodermis of the crayfish *Procambarus clarkii* during premolt. J Exp Biol 217:4193–4202. https://doi.org/10.1242/jeb.109009
77. Vivier D, Bennis K, Lesage F, Ducki S (2016) Perspectives on the two-pore domain potassium channel TREK-1 (TWIK-related K+ channel 1): a novel therapeutic target. J Med Chem 59:5149–5157. https://doi.org/10.1021/acs.jmedchem.5b00671
78. Waterhouse A, Bertoni M, Bienert S, Studer G, Tauriello G, Gumienny R, Heer FT, de Beer TAP, Rempfer C, Bordoli L, Lepore R, Schwede T (2018) SWISS-MODEL: homology modelling of protein structures and complexes. Nucleic Acids Res W296–W303 46(Web Server issue). https://doi.org/10.1093/nar/gky427
79. Wang Y, Xu D, Guo C, Zhang T, Liu J, Li W (2025) Gonadal development and its influencing factors in the red swamp crayfish (*Procambarus clarkii*): a review. Biology 14:1138. https://doi.org/10.3390/biology14091138
80. Zúñiga L, Zúñiga R (2016) Understanding the cap structure in K2P channels. Front Physiol 7:228. https://doi.org/10.3389/fphys.2016.00228

Figures

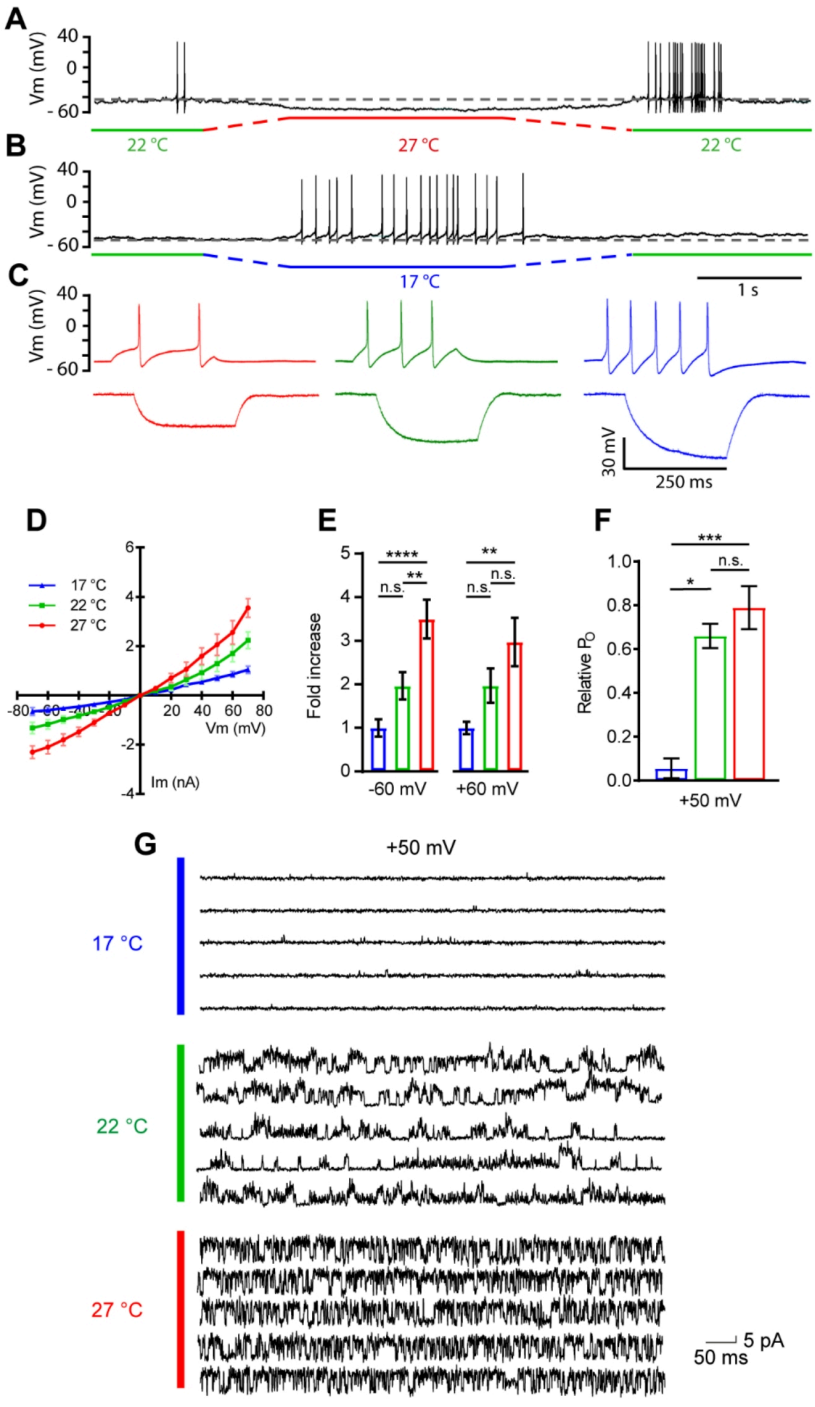


Figure 1

Temperature activates a background K⁺ leak conductance in X-organ neurons. A. Representative current-clamp recording from an X-organ neuron showing hyperpolarization of the membrane potential from −44 to −56 mV when temperature increased from 22 to 27 °C; the potential returned to baseline when temperature was lowered back to 22 °C. **B.** Representative current-clamp recording showing depolarization of the membrane potential from −50 to −44 mV when temperature was decreased from

22 to 17 °C, promoting neuronal activity; the potential was restored upon return to 22 °C. **C.** Representative voltage responses after current injection from an X-organ neuron shows the effects of the three temperature conditions: top traces show voltage responses after depolarization pulse, and bottom traces show corresponding changes in membrane voltage after hyperpolarization pulse. **D.** Current–voltage (I–V) relationship of average whole-cell recordings from X-organ neurons at three different temperatures. Currents were recorded in symmetrical K^+ solution using a square-pulse protocol (–70 to +70 mV in 10 mV steps, 1 s duration) from 0 mV holding potential. Data are expressed as mean ± SEM (n = 10). **E.** Temperature-dependent stimulation of current amplitude, expressed as fold increase relative to 17 °C (I_T / I_17°C) at –60 and +60 mV. From 17 to 27 °C, current amplitude increased 3.5-fold at –60 mV and 2.97-fold at +60 mV (ns, not significant; **p < 0.01; ****p < 0.0001). **F.** Open probability (Po) at 50 mV (ns, not significant; **p < 0.01; ****p < 0.0001). **G.** Representative single-channel recordings from an X-organ neuron at 50 mV under the three temperature conditions.

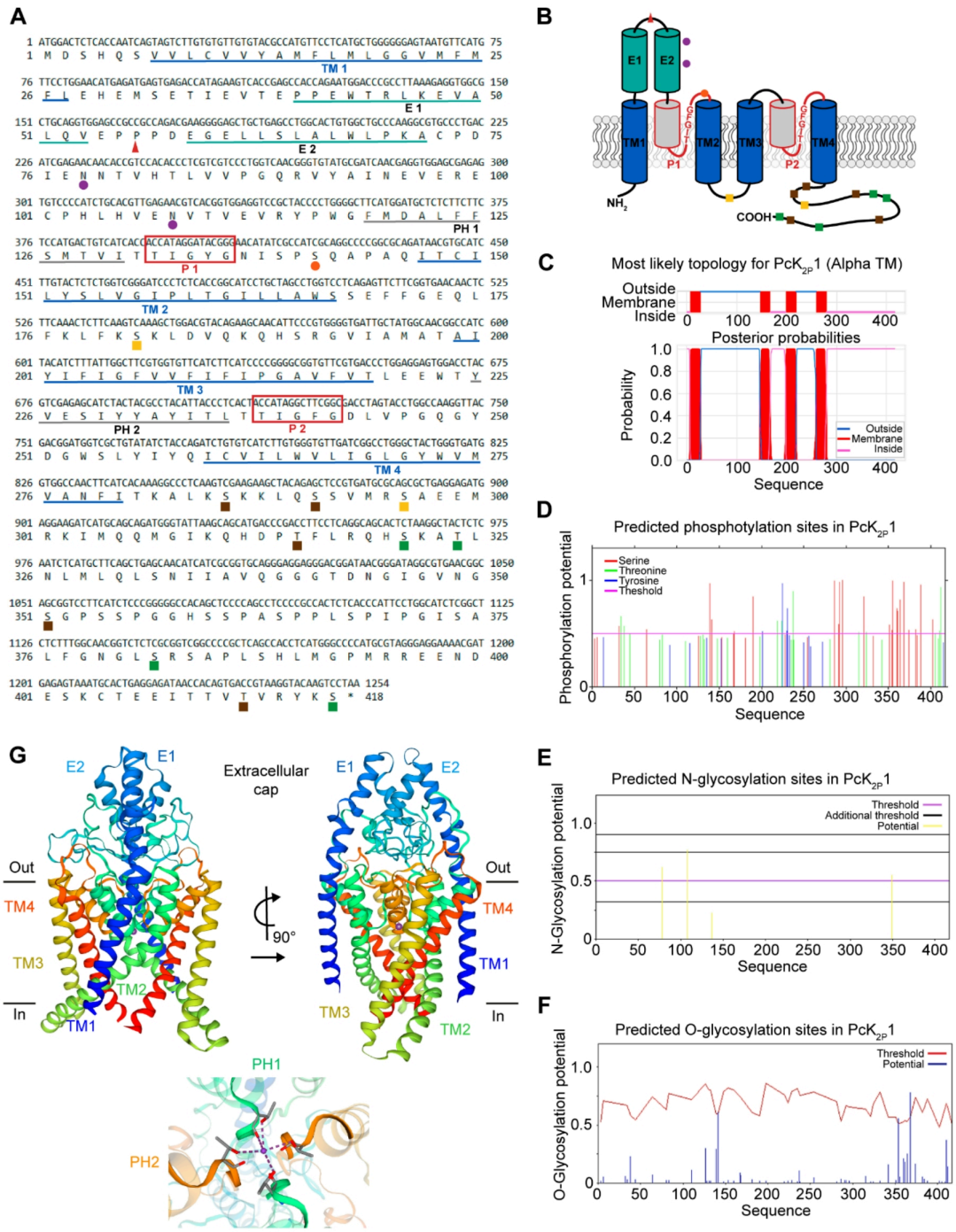


Figure 2

Bioinformatic analysis of $PcK_{2P}1$. A. The full-length $PcK_{2P}1$ ORF comprises 1,254 nucleotides and encodes a protein of 417 amino acids. The four predicted transmembrane helices (TM1–TM4) are underlined in blue, and the two selectivity filter motifs (P1 and P2) are boxed in red. The two predicted extracellular helices (E1 and E2) are underlined in turquoise, and the two pore helices (PH1 and PH2) are underlined in gray. Predicted O-linked and N-linked glycosylation sites are marked with purple and orange

circles, respectively. Predicted phosphorylation sites for PKA, PKC, and CKII are indicated by green, brown, and yellow squares, respectively. **B.** Predicted membrane topology of the $PcK_{2P}1$ subunit, showing the structural features and predicted modification sites described in A. **C.** Most likely membrane topology of $PcK_{2P}1$, comprising four transmembrane helices, a short cytoplasmic N-terminus, a long cytoplasmic C-terminus, and an extended extracellular region between TM1 and TM2. **D.** Predicted phosphorylation sites, with distinct colors indicating sites associated with different kinases. **E.** Predicted N-linked glycosylation sites. **F.** Predicted O-linked glycosylation sites. **G.** Homology model of $PcK_{2P}1$ generated using the human TREK-2 structure (PDB: 4XDL) as a template. Each subunit is colored from blue at the N-terminus to red at TM4. The C-terminal region could not be modeled and is therefore omitted. The K^+ ion is shown as a purple sphere, and horizontal lines indicate the approximate boundaries of the lipid membrane. The central cavity lies immediately below the K^+ ion along the symmetry axis. The right panel shows an orthogonal side view of the channel. The bottom panel shows an enlarged view of the predicted pore region, highlighting conserved threonine residues corresponding to those involved in K^+ coordination in the TREK-2 template.

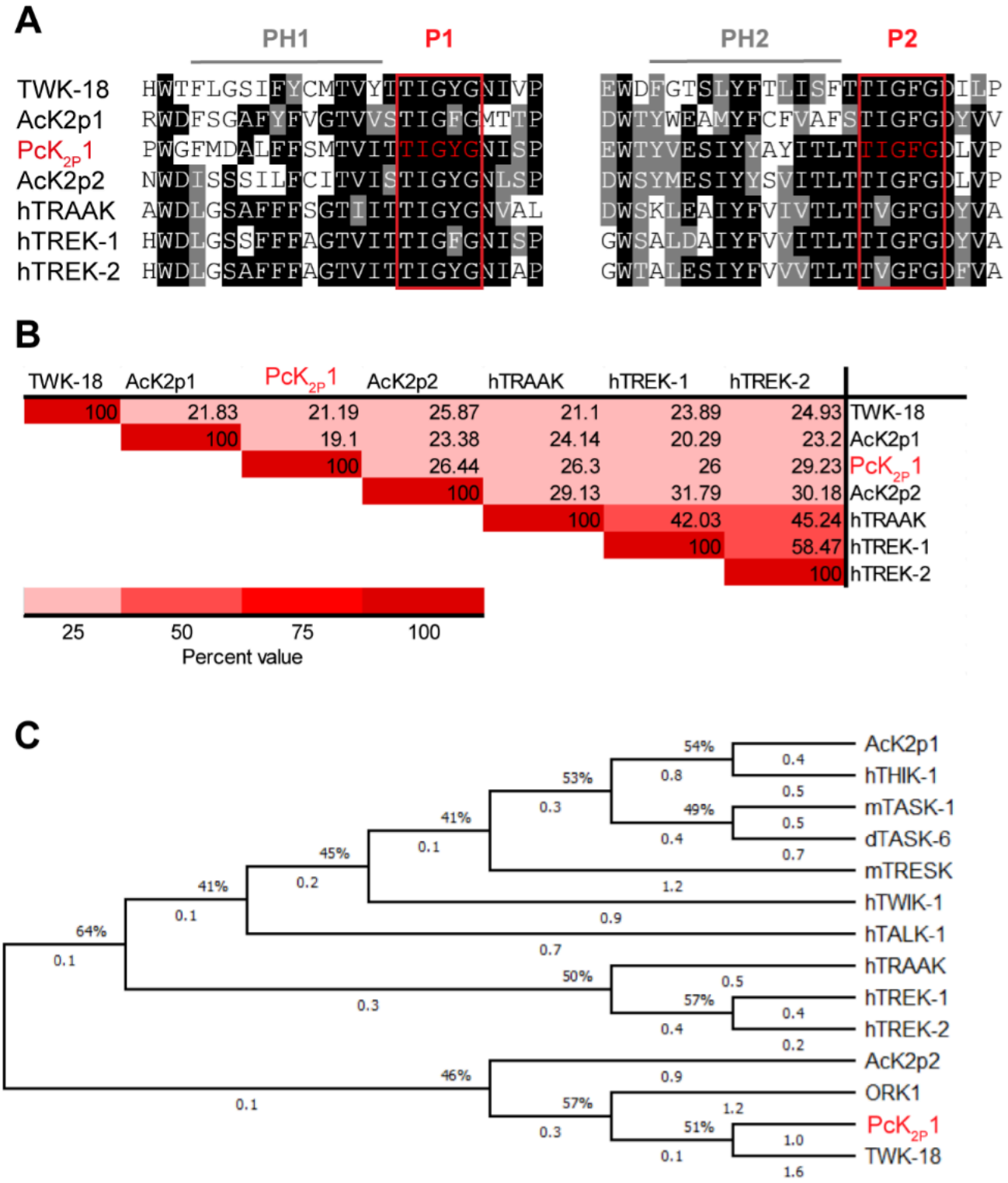


Figure 3

Sequence and phylogenetic analysis of the $PcK_{2P}1$ subunit. A. Alignment of $PcK_{2P}1$ regions. Potassium selectivity filter motifs (P1 and P2, red boxes) and pore helices (PH1 and PH2, gray line) from $PcK_{2P}1$ and other K_{2P} channel subunits; $PcK_{2P}1$ is highlighted in red letters. P1 and P2 show high sequence identity within both vertebrate and invertebrate K_{2P} members, including C. elegans TWK-18 (Q18120), *Aplysia californica* AcK2p1 (AAN62847.1) and AcK2p2 (DQ166529.1), as well as human TRAAK

(Q9NYG8), TREK-1 (O95069), and TREK-2 (P57789). Identical and similar residues are highlighted in black and gray, respectively. ***B.*** Pairwise identity matrix showing sequence similarity between $PcK_{2P}1$ and selected K_{2P} subunits. Each box displays the percentage of shared identity between subunits. ***C.*** Phylogenetic tree showing the evolutionary relationships of $PcK_{2P}1$ with other K_{2P} channels. The tree was inferred using the Maximum Likelihood method and the JTT matrix-based model. $PcK_{2P}1$ (red circle) clusters with invertebrate K_{2P} subunits and is part of a branch closely related to the human TREK subfamily.

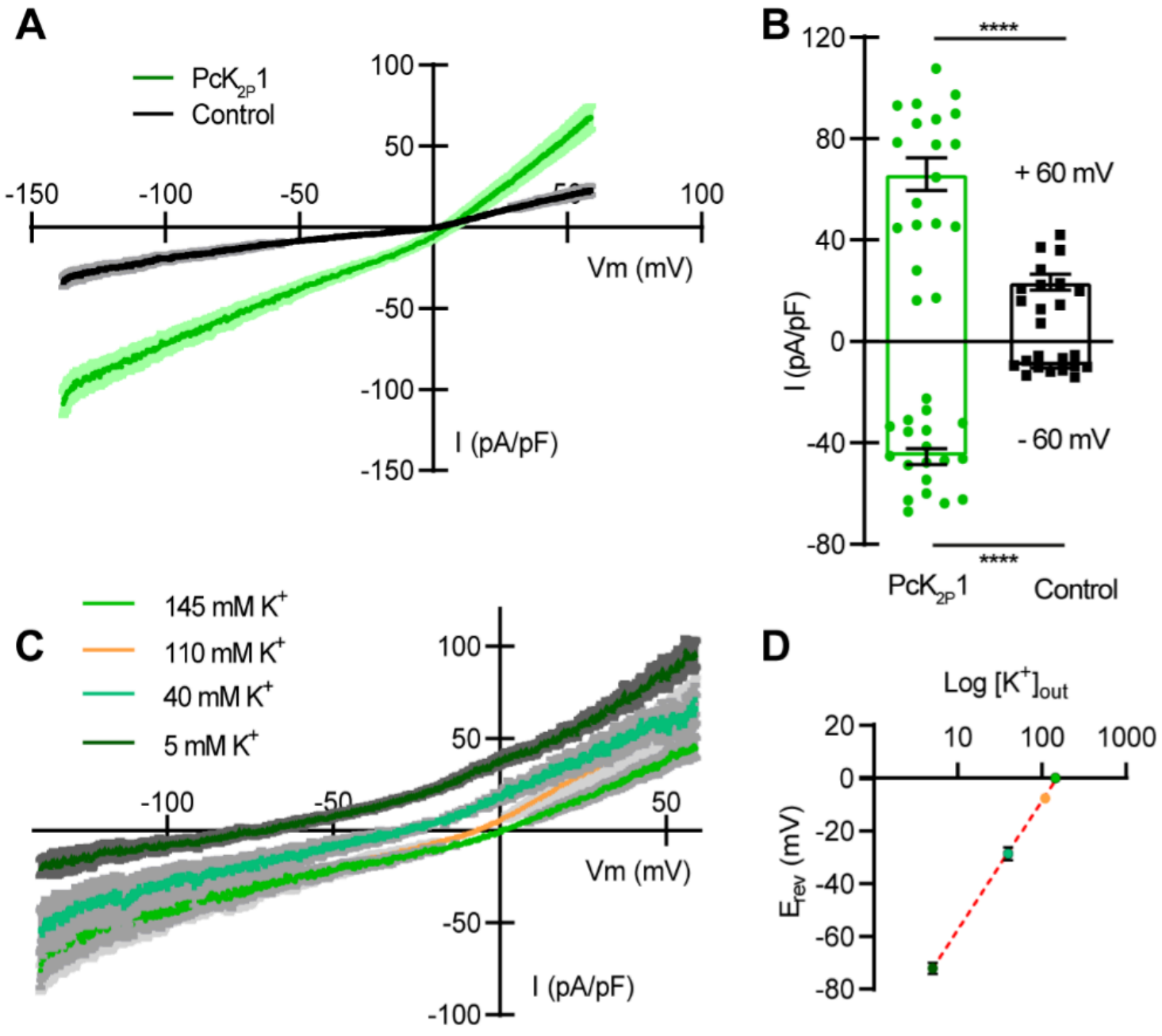


Figure 4

Functional properties of $PcK_{2P}1$ expressed in HEK293T cells. A. Current-voltage relationship in whole cell configuration from HEK293T cells either transfected with $PcK_{2P}1$ (green) or not transfected (black). Currents were recorded in 145 mM potassium solution using a voltage ramp protocol from −140 to +60 mV, 0 mV Vh, 1 s duration. Average current values are shown as pA/pF, mean ± SEM., n = 21 and n = 13 for transfected and non-transfected cells, respectively. **B.** Quantification of normalized current amplitude at −60 and + 60 mV in HEK293T transfected with $PcK_{2P}1$ (green) and without transfection (black) (current shown as pA/pF, mean ± SEM; **** $p < 0.0001$). **C.** Current-voltage relationship of HEK293T cells transfected with $PcK_{2P}1$ under four extracellular potassium conditions: 145 mM K^+ (n = 9; green), 110 mM K^+ (n = 7; orange), 40 mM K^+ (n = 4; light green) and 5 mM K^+ (n = 9; dark green). **D.** Plot of reversal potential of $PcK_{2P}1$ currents obtained at various extracellular potassium concentrations.

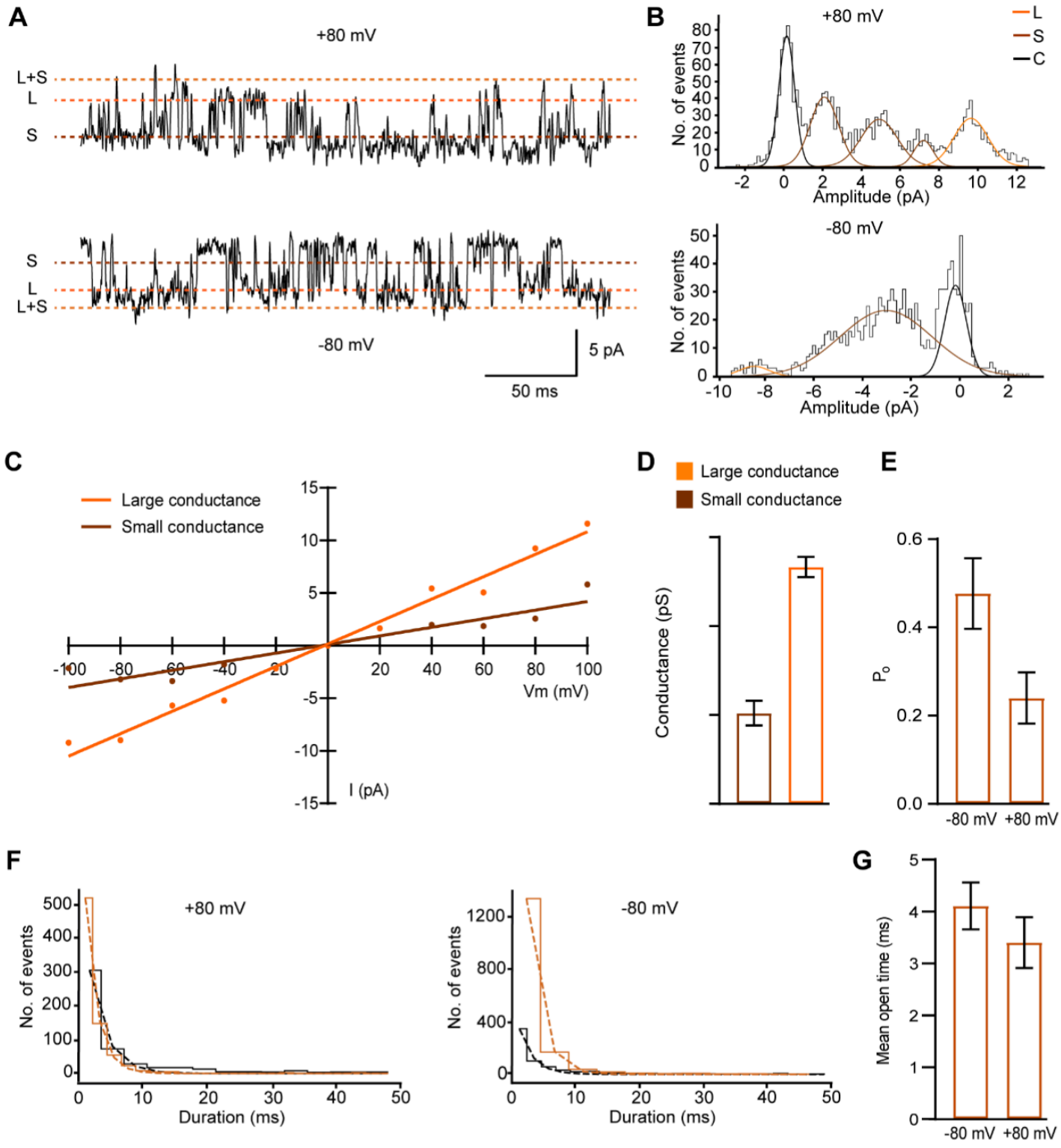


Figure 5

Single-channel properties of PcK$_{2P}$1 expressed in HEK293T cells. A. PcK$_{2P}$1 channel openings at +80 and −80 mV; S and L indicate small and large conductance levels, respectively, denoted by dotted lines. **B.** Channel openings were recorded at −80 and +80 mV and analyzed to obtain amplitude histograms. Gaussian fit of the conductance level distribution, where the colors black, brown, and orange indicate closed, small, and large conductance, respectively. ***C.*** Current-voltage relationship of small and large

conductance obtained from recordings of cell membrane patches maintained at pipette potentials of +100 to −100 mV. Pipette and bath solution contained 140 mM KCl. **D.** Unitary conductance for $PcK_{2P}1$. **E.** Open probability was analyzed at −80 and +80 mV. **F.** Duration histograms fitted using a single exponential function analyzed at −80 and +80 mV. **G.** Mean open time for $PcK_{2P}1$ at −80 and +80 mV. Data are shown as mean ± SEM of 20 cells analyzed.

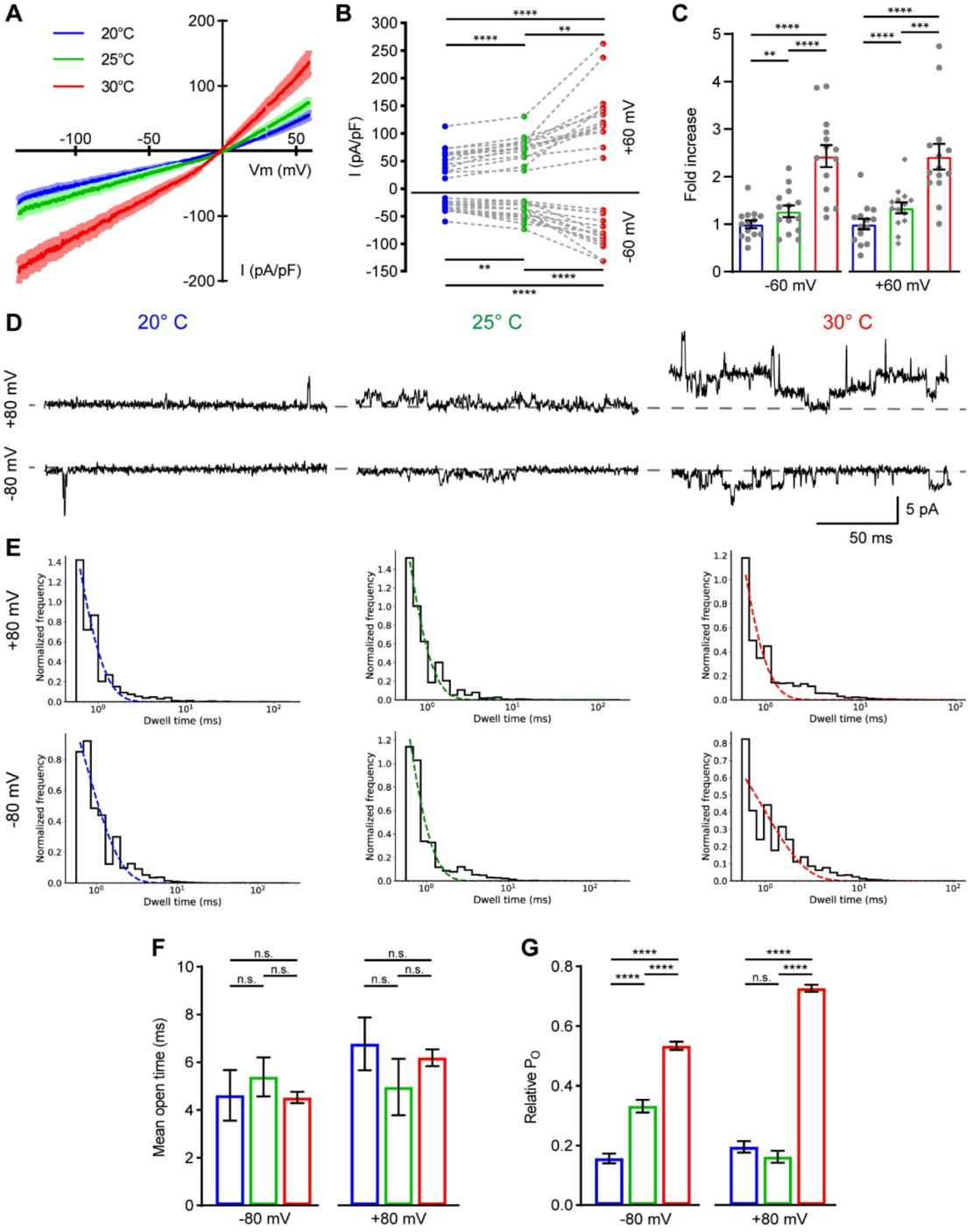


Figure 6

Heat modulation of $PcK_{2P}1$ expressed in HEK293T cells. A. Current–voltage (I–V) relationships from whole-cell recordings of HEK293T cells transfected with $PcK_{2P}1$ under three different temperature conditions. Currents were recorded in symmetrical K^+ solution using a voltage-ramp protocol (–140 to +60 mV, 1 s) at 0 mV Vh. Values are expressed as pA/pF (mean ± SEM, n = 14). **B.** Dot plots of normalized current amplitudes at –60 and +60 mV. Each dot represents an individual cell at the indicated temperature (**$p < 0.01$, ****$p < 0.0001$). **C.** Temperature-dependent stimulation of current amplitude, expressed as fold increase relative to 20 °C (I_T / I_20 °C) at –60 and +60 mV. From 20 to 30 °C, current amplitude increased 2.43-fold at –60 mV and 2.42-fold at +60 mV (**$p < 0.01$, ***$p < 0.001$, ****$p < 0.0001$). **D.** Representative single-channel recordings of $PcK_{2P}1$ at +80 and –80 mV under the three temperature conditions. A dashed line indicates the closed level. **E.** Open-time histograms fitted with a single-exponential function, obtained from ~10 s of recordings at –80 and +80 mV under the three temperature conditions. **F.** Mean open time of $PcK_{2P}1$ at –80 and +80 mV (mean ± SEM; ns, not significant). **G.** Relative open probability (P_o) at –80 and +80 mV (ns, not significant; ****$p < 0.0001$).

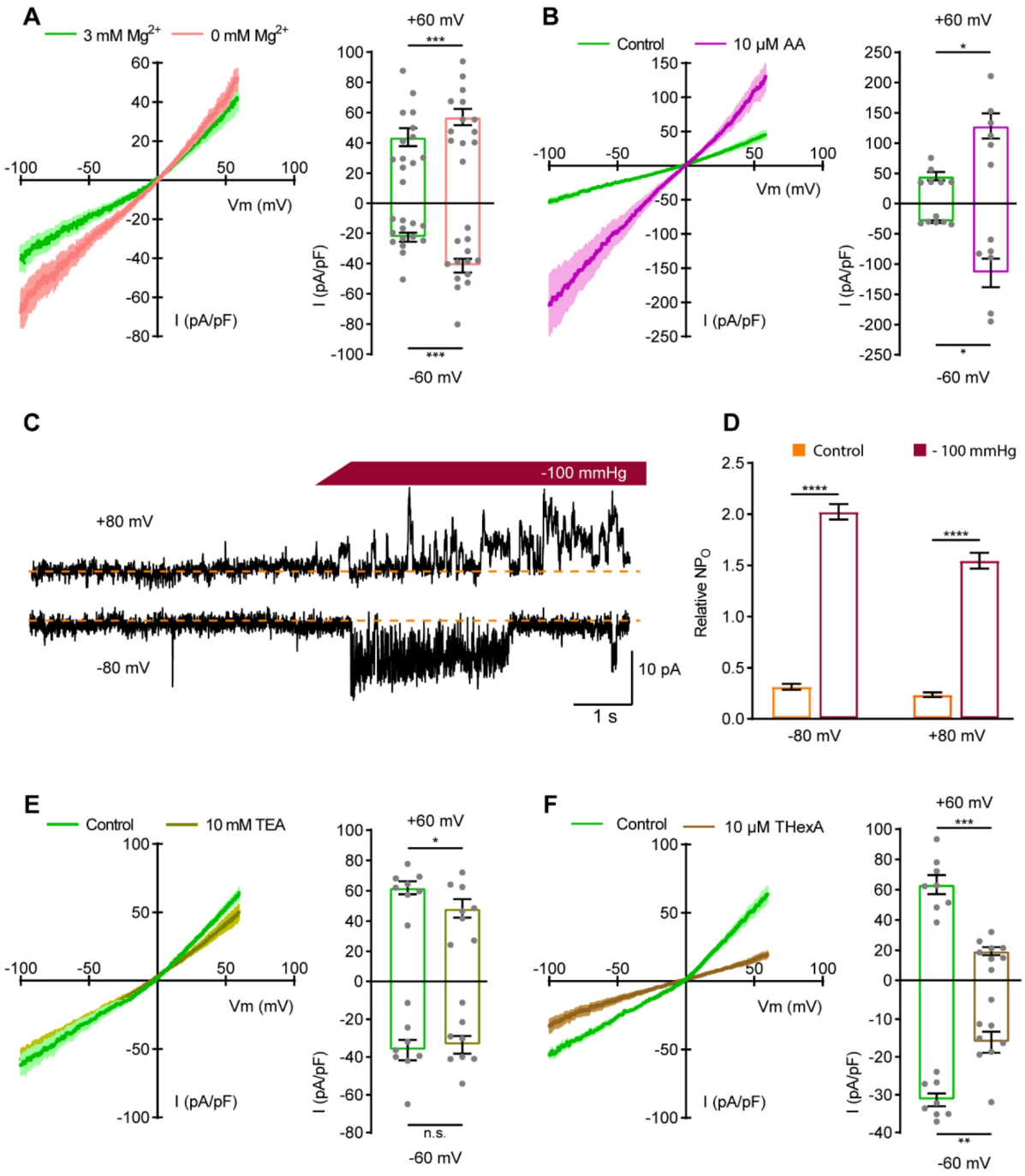


Figure 7

Modulation of $PcK_{2P}1$ expressed in HEK293T cells. Currents were recorded in symmetrical 145 mM potassium solution using a voltage ramp protocol from −100 to +60 mV, from a 0 mV Vh, with a 1 s of duration. Data are shown as pA/pF (mean ± SEM). **A.** Left, current–voltage relationship of average whole-cell recordings of $PcK_{2P}1$ in the presence of 3 mM Mg^{2+} (green) and in the absence of Mg^{2+} (peach). Right, quantification of current amplitudes normalized at −60 and +60 mV; each gray circle

represents one recorded cell (n = 13 per condition; ***p < 0.001). **B.** Left, current–voltage relationship of average whole-cell recordings of $PcK_{2P}1$ in control symmetrical K^+ solution (green) and in the presence of 10 μM arachidonic acid (AA, purple). Right, quantification of current amplitudes normalized at –60 and +60 mV; each gray circle represents one recorded cell (n = 6 per condition; *p < 0.1.) **C.** Representative single-channel recordings of $PcK_{2P}1$ at +80 and –80 mV under atmospheric pressure and during –100 mmHg negative pressure (wine-colored bar). The dashed line indicates the closed level. **D.** Relative activity (NPo) at –80 and +80 mV (****p < 0.0001). **E.** Left, current–voltage relationship of average whole-cell recordings of $PcK_{2P}1$ in control symmetrical solution (green) and in the presence of 10 mM tetraethylammonium (TEA, dark green). Right, quantification of normalized current amplitudes at –60 and +60 mV; each gray circle represents one recorded cell (n = 8 per condition; ns, not significant; *p < 0.05). **F.** Left, current–voltage relationship of average whole-cell recordings of $PcK_{2P}1$ in control symmetrical solution (green) and in the presence of 10 μM tetrahexylammonium (THexA, brown). Right, quantification of normalized current amplitudes at –60 and +60 mV; each gray circle represents one recorded cell (n = 8 per condition; ns, not significant; **p < 0.01, ***p < 0.001).

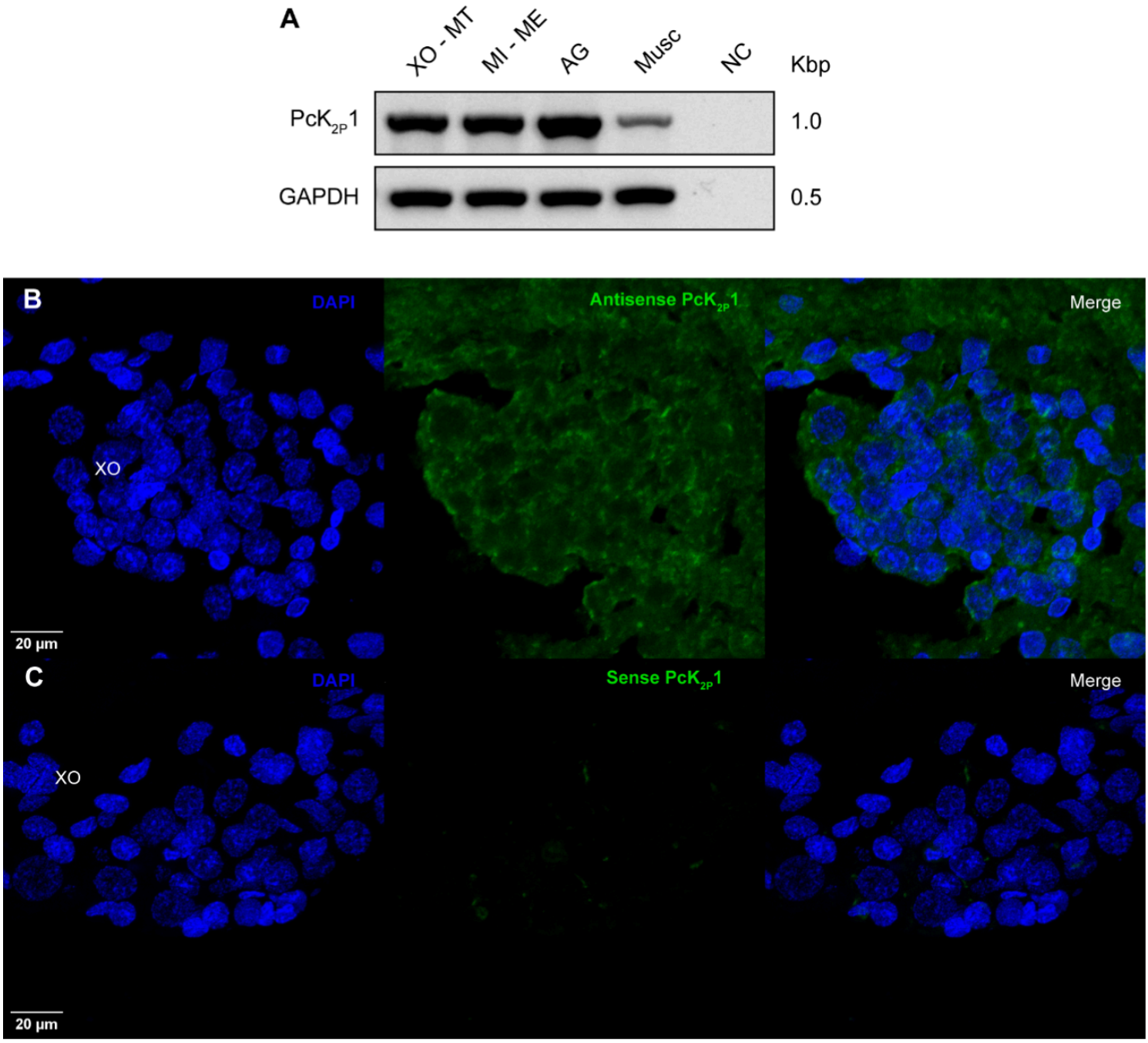


Figure 8

Expression of $PcK_{2P}1$ in the eyestalk of *P. clarkii*. A. Agarose gel electrophoresis showing expression of the $PcK_{2P}1$ subunit (1.0 kbp) in different tissues. $PcK_{2P}1$ cDNA was detected in all tissues analyzed. XO-MT, X-organ–medulla terminalis; MI–ME, medulla interna–medulla externa; AG, abdominal ganglia; Musc, muscle tissue; NC, negative control. **B.** Fluorescent *in situ* hybridization (FISH) using an antisense riboprobe against $PcK_{2P}1$ revealed abundant mRNA expression in neurons of the X-organ (XO). ***C.*** Negative control hybridization performed with the sense riboprobe showed no detectable signal.